NATIONAL ADVISORY COMMITTEE
FOR AERONAUTICS

TECHNICAL NOTE 2000

DATA ON SHAPE AND LOCATION OF DETACHED SHOCK WAVES

ON CONES AND SPHERES

By Juergen W. Heberle, George P. Wood,
and Paul B. Gooderum

Langley Aeronautical Laboratory
Langley Air Force Base, Va.

Washington

January 1950

20000801 083

DTIC QUALITY INSPECTED 4

AQM 00-10-3376

NATIONAL ADVISORY COMMITTEE FOR AERONAUTICS

TECHNICAL NOTE 2000

DATA ON SHAPE AND LOCATION OF DETACHED SHOCK WAVES

ON CONES AND SPHERES

By Juergen W. Heberle, George P. Wood,
and Paul B. Gooderum

SUMMARY

Accurate experimental data are given on the shape and the location of detached shock waves on cones and spheres at Mach numbers from 1.17 to 1.81. The data are correlated to obtain equations that describe the shock waves. This knowledge of the shock waves should be useful in calculations of the pressure distribution and the pressure drag of the fore part of cones and spheres. The experimental data on shock waves are compared with theory.

INTRODUCTION

One of the problems in aerodynamics that is of current interest is the problem of predicting the shape and the location of detached shock waves, or bow waves. The problem is of practical importance because a knowledge of the shock wave is useful in calculating the drag of the nose of the body behind the shock wave. The flow behind a detached shock wave is subsonic in a region that is bounded by the shock wave, the sonic line, and the fore part of the body. If these boundaries of the subsonic region are known, then the pressure distribution over the fore part, or nose, of the body and the pressure drag of the fore part of the body can be calculated (references 1 and 2).

A few theoretical attacks on the problem of describing the detached shock waves on bodies of revolution have been made (references 3 to 6). Attempts have been made to compare the theoretical results with the available experimental results (references 3, 5, and 6). Experimental results have, however, been scarce.

The purpose of the present paper is to give experimental data on the location of detached shock waves on spheres and conical-tip cylinders. (For brevity, the conical-tip cylinders are referred to in the present paper as cones.) For this purpose, series of

interferograms were taken of the flow around spheres and cones, of
various vertex semiangles between 35° and 90°, at Mach numbers ranging
from 1.17 to 1.81. Measurements of the shock waves were made on these
interferograms and were correlated to obtain equations that describe
the part of the shock wave ahead of the sonic line.

SYMBOLS

$c_0, c_1, c_2, \ldots$	coefficients
C	constant of apparatus
d	diameter of sphere; diameter of cylinder
K	curvature of bow wave at its nose
M	free-stream Mach number
n	number of points measured on a bow wave
p	pressure of air in jet
R	gas constant
s_1	axial distance of shock wave from center of sphere
s_2	axial distance of shock wave from plane of shoulder of cone
S	fringe shift in free stream
T	static temperature of air in jet
T_s	stagnation temperature of air in jet

x, y	coordinates
X	dimensionless coordinate (x/d)
Y	dimensionless coordinate (y/d)
γ	ratio of specific heats
$\bar{\delta}$	root-mean-square deviation
ρ_a	density of atmospheric air
ρ	density of air in jet
θ	vertex semiangle of conical tip

APPARATUS

A 3-inch-square free jet and an interferometer with 4-inch-square plates were used. This apparatus has been described in reference 7. Different Mach numbers were obtained by using five supersonic nozzles similar to those described in reference 7. For the calibration of each nozzle, interferograms were taken that showed part of the free stream and also part of the undisturbed region outside the jet. The fringe shift S in the free stream was determined by comparing such an interferogram with a no-flow interferogram. Then the free-stream density ρ was computed by means of equation (3) of reference 7,

$$\frac{\rho}{\rho_a} = CS + 1$$

where C is a constant of the apparatus and where ρ_a, the density of the undisturbed air, was determined from the measured atmospheric pressure and temperature. The supply to the jet was regulated in such a way that the jet emerged with its static pressure equal to that of the atmosphere. Then, the static temperature T in the free stream was computed by the general gas law,

$$p = \rho RT$$

The stagnation temperature T_S was measured with a thermocouple a short distance upstream of the nozzle where the airspeed was low. Then the Mach number was obtained from the relation

$$\frac{T_S}{T} = 1 + \frac{\gamma - 1}{2}M^2$$

The calibration yielded the values 1.17, 1.30, 1.37, 1.62, and 1.81 for the Mach numbers of the five nozzles. The determination of the Mach number given by each nozzle was made as carefully as was practicable. Some uncertainty, nevertheless, exists in the final result. This uncertainty is estimated to be not greater than 3 percent.

RESULTS

Spheres

Interferograms of the flow at several Mach numbers around spheres of various diameters d are shown in figures 1 to 5. Additional interferograms with spheres of other diameters were taken at each Mach number. At a given Mach number, corresponding distances on different interferograms were found to be proportional to d; that is, in these tests, the Reynolds number had no apparent effect on the part of the shock wave that was ahead of the sonic line. Therefore, only one interferogram is shown for each Mach number except for Mach number 1.81, for which interferograms of the flow around spheres of three different diameters have been included to illustrate this result (fig. 5).

Axial distance of shock waves.- The axial distance s_1 of the shock wave from the center of the sphere has been obtained from figures 1 to 5. The variation of the quantity s_1/d with Mach number is shown in figure 6. The equation of the curve that has been drawn through the experimental points is

$$\frac{s_1}{d} = \frac{2}{3}(M - 1)^{-1/3} \qquad\qquad (1)$$

Over the range of Mach number used, the curve fits the data well. Equation (1) is not applicable, however, at Mach numbers much greater than the largest used in the present tests, because, according to equation (1), the distance between the nose of the shock wave and the center of the sphere is less than the radius of the sphere at Mach numbers greater than 3.37.

Whether equation (1) remains applicable at Mach numbers less than the smallest used in the present investigation is not yet known. The equation does give, however, the correct asymptotic value, infinity, for the quantity s_1/d as the Mach number approaches unity.

The theory of reference 3 predicts the variation of the distance between the nose of the shock wave and the nose of the sphere, $\dfrac{s_1}{d} - \dfrac{1}{2}$, with Mach number, for Mach numbers near unity. A comparison of the theoretical results with the present experimental results is given in figure 7. One of the curves in figure 7 is taken from figure 2 of reference 3. The curve for the experimental results is plotted from equation (1) of the present paper. Reference 6 also predicts the location of the shock wave. One of the curves in figure 7 is based on the results of reference 6.

Equations of shock waves.- Equations for that part of the shock wave which bounds the subsonic region have also been determined. The coordinates x and y of points on the shock wave were measured with reference to the axes shown in the adjacent sketch. The measurements were reduced to the dimensionless variables

$$X = \frac{x}{d}$$

$$Y = \frac{y}{d}$$

The results of these measurements are given in table I.
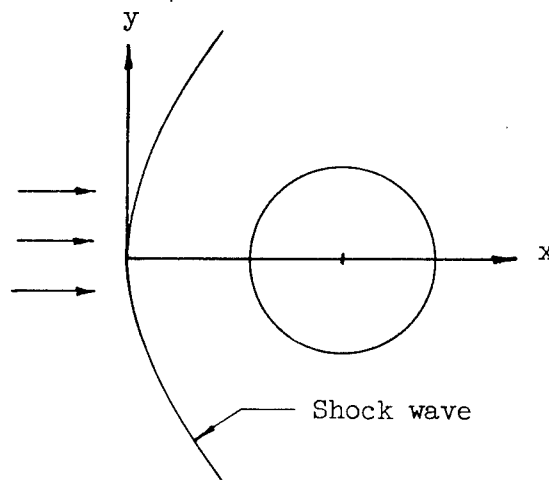
The simple shape of the shock wave suggests the use of a power series

$$X = c_0 + c_1 Y + c_2 Y^2 + c_3 Y^3 + c_4 Y^4 + c_5 Y^5 + c_6 Y^6 + \ldots$$

to describe it. Because of the choice of the origin and because the shock wave is symmetrical about the x-axis,

$$c_0 = c_1 = c_3 = c_5 = \ldots = 0$$

and, therefore,

$$X = c_2 Y^2 + c_4 Y^4 + c_6 Y^6 + \ldots \tag{2}$$

The first two terms on the right-hand side of the equation are found to be sufficient for an accurate description of the shock waves.

Application of the method of least squares yields the following formulas for the coefficients:

$$c_2 = \frac{1}{D} \left(\sum X_i Y_i^2 \sum Y_i^8 - \sum X_i Y_i^4 \sum Y_i^6 \right)$$

$$c_4 = -\frac{1}{D} \left(\sum X_i Y_i^2 \sum Y_i^6 - \sum X_i Y_i^4 \sum Y_i^4 \right)$$

where $i = 1, 2, 3, \ldots n$, the values of X_i and Y_i are taken from table I, and

$$D = \sum Y_i^4 \sum Y_i^8 - \left(\sum Y_i^6 \right)^2$$

Associated with each pair of values c_2 and c_4 is the quantity

$$\bar{\delta} = \left(\sum_{i=1}^{n} \frac{\delta_i^2}{n} \right)^{1/2}$$

where $\delta_i = c_2 Y_i^2 + c_4 Y_i^4 - X_i$. The value of $\bar{\delta}$ is a measure of how well the equation fits the data; the smaller $\bar{\delta}$ is, the better the fit.

Computed values of c_2, c_4, and $\bar{\delta}$ are listed in table II. In figure 8, these values of c_2 and c_4 are plotted against M.

An inspection of the figure shows that there is a fairly regular variation of c_2 and c_4 with Mach number. Curves that show the approximate variation have been arbitrarily drawn in figure 8 to aid in interpolation at other than test Mach numbers. The equations of these curves are

$$c_2 = 1 - e^{-0.70(M-1)} \tag{3}$$

$$c_4 = -0.042(M - 1) \tag{4}$$

The scatter in the values of c_4 is much larger, on a relative basis, than the scatter in the values of c_2. This large uncertainty in the value of c_4 does not necessarily indicate a large uncertainty, however, in the values of X calculated from equations (2), (3), and (4), because the term in equation (2) that contains c_4 is usually much smaller than the term that contains c_2.

Curvature of shock waves.- Reference 5 is a theoretical investigation of the problem of the detached shock wave in front of a body of revolution. One of the quantities that is studied is the product $\left(s_1 - \dfrac{d}{2}\right)K$, where $s_1 - \dfrac{d}{2}$ is the distance of the nose of the shock wave from the nose of the sphere and K is the curvature of the shock wave at its nose. Two approximations to the variation of $\left(s_1 - \dfrac{d}{2}\right)K$ with Mach number are derived. See equations (29) and (30) of reference 5. These equations have been used to plot the curves shown in figure 9. These theoretical results can be compared with the present experimental results. The curvature K is easily shown from equation (2) to be $2c_2/d$. Experimental values of the product $\left(s_1 - \dfrac{d}{2}\right)K$ have been computed from the values of c_2 in table II and the values of s_1/d in figure 6. These experimental values are shown in figure 9.

Location of sonic line.- For calculation of the pressure drag by the method of reference 1, a knowledge of at least the approximate location of the sonic line, as well as the shock wave, is needed. The two ends of the sonic line can be located fairly accurately from the results given in the present paper. The location of the end of the sonic line that lies on the shock wave can be found from the equation

of the shock wave, equation (2), and the simple theory of oblique shock waves, which gives the angle of the shock wave for which the Mach number immediately behind the shock wave is unity.

The position of the other end of the sonic line, at the surface of the sphere, can be obtained approximately from information that has been obtained in connection with another investigation. Interferograms of the flow around spheres at Mach numbers of 1.30 and 1.62 were analyzed sufficiently to locate the end of the sonic line. The sonic line was found to intersect the sphere 48° from the nose of the sphere at a Mach number of 1.30 and 52° from the nose at a Mach number of 1.62. Over at least most of the range of Mach number covered in the present paper, therefore, the end of the sonic line is close to 50° from the nose of the sphere.

Cones

A set of conical-tip cylinders was fabricated from steel rods of various diameters by machining one end to the shape of cones with various vertex angles. The circle of intersection of the conical part with the cylindrical part is referred to as the shoulder of the cone. Interferograms of the flow around these cones at various Mach numbers were taken and are shown as figures 10 to 15.

Axial distance of shock waves.- The axial distance s_2 of the shock wave from the plane of the shoulder was measured on the interferograms. The ratio s_2/d is shown in figure 16 as a function of Mach number. A simple equation that describes the variation of s_2/d with Mach number over the range of the experiments was obtained from the data. The equation is

$$\frac{s_2}{d} = 0.48(M - 1)^{-1/2} \tag{5}$$

and was used to plot the curve shown in figure 16.

Although a wide range of vertex angle was used, s_2/d does not vary much with vertex angle at a given Mach number. The variation in s_2/d with angle does not exceed about 10 percent. This result was true even when the vertex semiangle was increased to 90° and the end of the cylinder thus became flat. This result agrees with Busemann's result (reference 8), which is stated for two-dimensional flow but which should be true also for three-dimensional flow, that the shoulder is the most important part of a body in determining the detached shock wave and that the nose is unimportant in the determination of the location of the detached shock wave.

The result that the cone angle had little effect on the value of s_2/d was not true when the cone angle was decreased enough for the shock wave to approach attachment to the tip of the cone. A typical case when the shock wave is nearly attached is shown in figure 15. The distance s_2 given by equation (5) does not apply in this case.

Equations of shock waves.- Measured values of the coordinates of the shock waves are given in table III. In a manner similar to that used for the spheres, a power series

$$X = c_2 Y^2 + c_4 Y^4$$

was fitted to the shock waves on the cones. Computed values of the coefficients c_2 and c_4 and of the root-mean-square deviation $\overline{\delta}$ are listed in table IV.

Location of sonic line.- As was the case for spheres, the two ends of the sonic line can be located. The end that lies on the shock wave can be found from the theory of oblique shock waves. The other end lies at the shoulder of the body and is perpendicular to the surface of the conical tip (reference 2).

CONCLUDING REMARKS

Data have been obtained on the shape and the location of detached shock waves on spheres and cones. These data have been correlated to give equations that describe the shock waves. Information about the location of the sonic line has also been given. With the boundaries of the subsonic region behind the detached shock wave thus known, the pressure distribution and the pressure drag of the fore part of spheres and cones can be calculated, as for example by the method of Maccoll.

The experimental data given herein should also be useful for comparison with the results of future developments in the theory of detached shock waves.

Langley Aeronautical Laboratory
        National Advisory Committee for Aeronautics
                Langley Air Force Base, Va., September 19, 1949

REFERENCES

1. Maccoll, J. W.: Investigation of Compressible Flow at Sonic Speeds.
      Theoretical Res. Rep. No. 7/46, Armament Res. Dept., British
      Ministry of Supply, Sept. 1946.

2. Drougge, Georg: The Flow around Conical Tips in the Upper Transsonic
      Range. Rep. No. 25, Aero. Res. Inst. of Sweden (Stockholm), 1948.

3. Laitone, Edmund V., and Pardee, Otway O'M.: Location of Detached
      Shock Wave in Front of a Body Moving at Supersonic Speeds.
      NACA RM A7B10, 1947.

4. Lin, C. C., and Rubinov, S. I.: On the Flow behind Curved Shocks.
      Jour. Math. and Phys., vol. XXVII, no. 2, July 1948, pp. 105-129.

5. Dugundji, John: An Investigation of the Detached Shock in Front of
      a Body of Revolution. Jour. Aero. Sci., vol. 15, no. 12,
      Dec. 1948, pp. 699-705.

6. Moeckel, W. E.: Approximate Method for Predicting Form and Location
      of Detached Shock Waves ahead of Plane or Axially Symmetric
      Bodies. NACA TN 1921, 1949.

7. Gooderum, Paul B., Wood, George P., and Brevoort, Maurice J.: Investi-
      gation with an Interferometer of the Turbulent Mixing of a Free
      Supersonic Jet. NACA TN 1857, 1949.

8. Busemann, Adolf: A Review of Analytical Methods for the Treatment
      of Flows with Detached Shocks. NACA TN 1858, 1949.

TABLE I.- COORDINATES OF SHOCK WAVES ON SPHERES

M	d (in.)	X														
		Y = 0.1	Y = 0.2	Y = 0.3	Y = 0.4	Y = 0.5	Y = 0.6	Y = 0.7	Y = 0.8	Y = 0.9	Y = 1.0	Y = 1.2	Y = 1.4	Y = 1.6	Y = 2.0	Y = 2.4
1.17	1/4		0.008		0.018		0.070		0.072			0.151		0.257	0.374	0.512
1.30	1/2		.009		.031		.080		.122		0.186	.254	0.330	.417		
1.37	1/2				.037				.138		.209	.291	.381	.477		
1.62	1/2	0.003	.013	0.031	.056	0.087	.120	0.165	.211	0.265						
1.81	1/4	.005	.018	.041	.067	.106	.151	.201	.261							
1.81	1/2	.004	.016	.038	.066	.104	.149	.201	.259							
1.81	1	.004	.016	.037	.067	.104	.149	.199	.258							

TABLE II.- VALUES OF c_2, c_4, AND $\bar{\delta}$ FOR SPHERES

M	d (in.)	c_2	c_4	$\bar{\delta}$
1.17	1/4	0.1090	-0.00357	3×10^{-3}
1.30	1/2	.1970	-.01361	2
1.37	1/2	.2240	-.01488	1
1.62	1/2	.3480	-.02663	1
1.81	1/4	.4330	-.04009	1
1.81	1/2	.4233	-.02886	.5
1.81	1	.4239	-.03279	.4

TABLE III.- COORDINATES OF SHOCK WAVES ON CONES

M	θ (deg)	d (in.)	X																	
			Y=0.1	Y=0.2	Y=0.3	Y=0.4	Y=0.5	Y=0.6	Y=0.7	Y=0.8	Y=0.9	Y=1.0	Y=1.2	Y=1.4	Y=1.5	Y=1.6	Y=1.8	Y=2.0	Y=2.1	Y=2.4
1.17	35	1/4			0.004			0.041			0.083		0.146		0.225		0.314		0.418	
1.30	35	3/4			.020			.074			.153		.246		.351		.474		.541	0.671
	45	9/16			.014			.059			.127		.214		.309		.418			
	45	3/4			.016			.059			.122		.212		.322		.437		.530	.665
	60	9/16			.011			.052			.115		.199		.299		.410			
1.37	35	9/16		0.014		0.051		.100		0.162		0.232	.313	0.398		0.491	.592			
	35	3/4			.030			.101			.196		.310		.440		.591			
	45	9/16		.007		.035		.072		.121		.180	.248	.329		.415	.511	0.607		
	45	3/4			.019			.070			.151		.253		.376		.527			
	60	9/16		.007		.025		.058		.104		.158	.222	.296		.375	.463	.560		
1.62	45	9/16		.018		.061		.120		.195		.286	.389							
	45	3/4		.016		.057		.117		.191		.279	.380							
	60	9/16		.010		.040		.086		.149		.230	.326							
1.81	45	9/16	0.007	.026	.051	.080	0.115	.155	0.199	.248	.301	.291								
	45	3/4	.009	.027	.052	.083	.118	.158	.200	.248	.299									
	60	9/16	.003	.012	.028	.048	.075	.106	.143	.187	.237									

TABLE IV.- VALUES OF c_2, c_4, AND δ FOR CONES

M	θ (deg)	d (in.)	c_2	c_4	δ ($\times 10^{-3}$)
1.17	35	1/4	0.1050	-0.00234	2
1.30	35	3/4	.1924	-.01454	6
1.30	45	9/16	.1514	-.00621	6
1.30	45	3/4	.1586	-.00728	2
1.30	60	9/16	.1430	-.00489	3
1.37	35	9/16	.2508	-.02181	9
1.37	35	3/4	.2473	-.02060	9
1.37	45	9/16	.1862	-.00873	4
1.37	45	3/4	.1869	-.00771	3
1.37	60	9/16	.1618	-.00560	2
1.62	45	9/16	.3411	-.05038	5
1.62	45	3/4	.3315	-.04790	4
1.62	60	9/16	.2402	-.00953	1
1.81	45	9/16	.4922	-.15538	5
1.81	45	3/4	.5070	-.17757	5
1.81	60	9/16	.2978	-.00703	.7

L-62130

Figure 1.- Interferogram of flow around sphere at Mach number 1.17.

$$d = \frac{1}{4} \text{ inch.}$$

L-62131

Figure 2.- Interferogram of flow around sphere at Mach number 1.30.

$d = \frac{1}{2}$ inch.
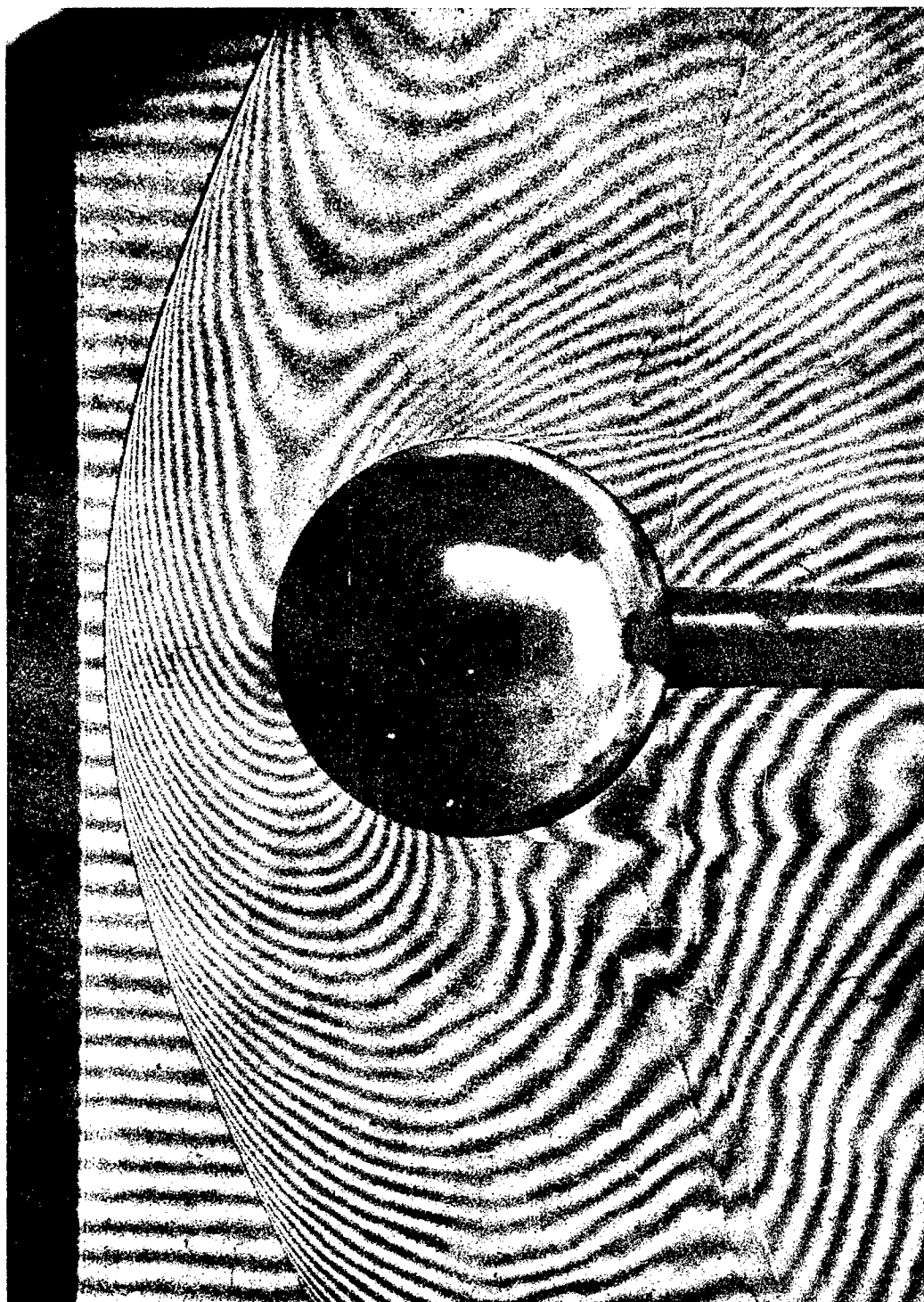
L-62132

Figure 3.- Interferogram of flow around sphere at Mach number 1.37. $d = \frac{1}{2}$ inch.
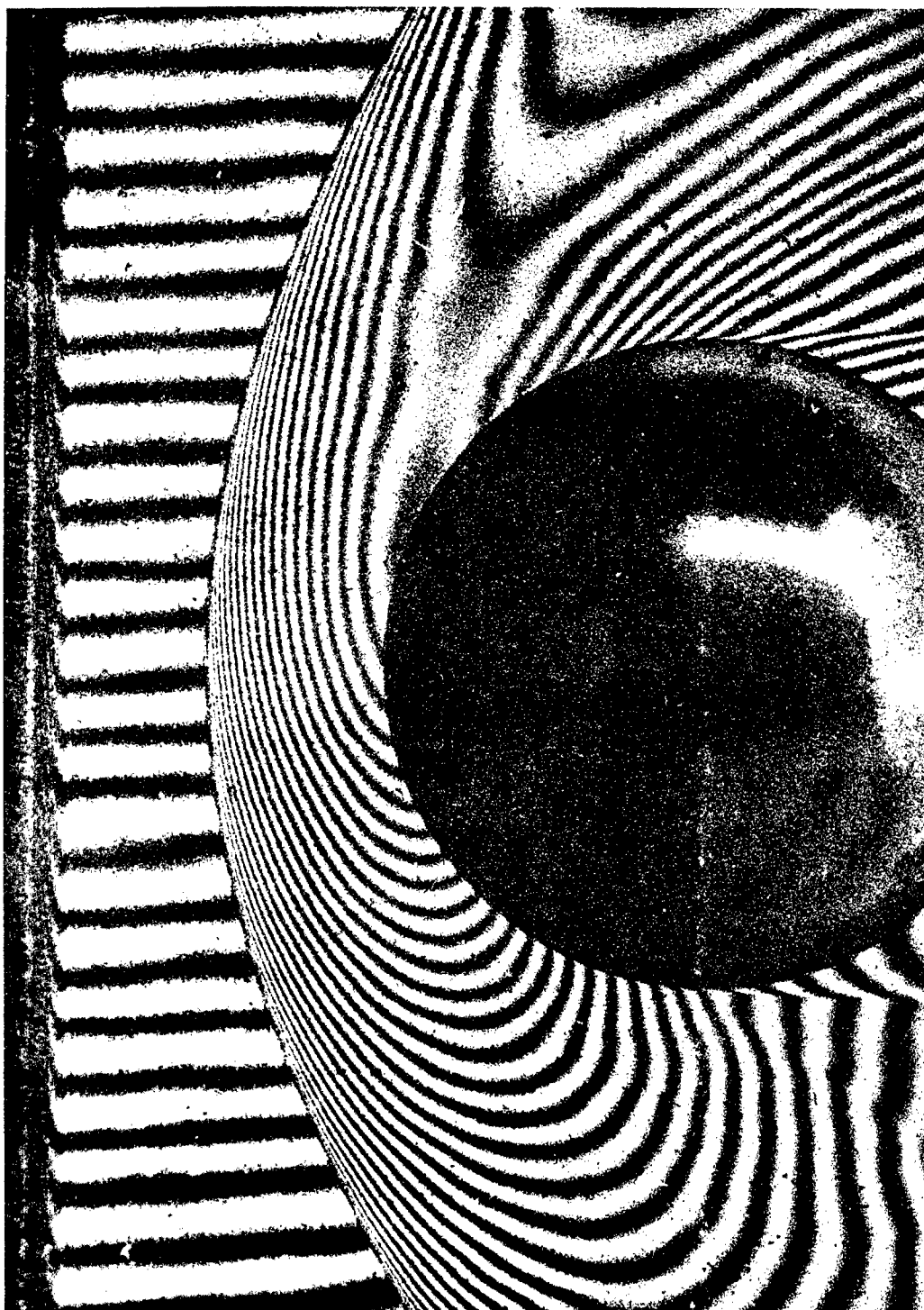
L-62133

Figure 4.- Interferogram of flow around sphere at Mach number 1.62.
$d = \frac{1}{2}$ inch.
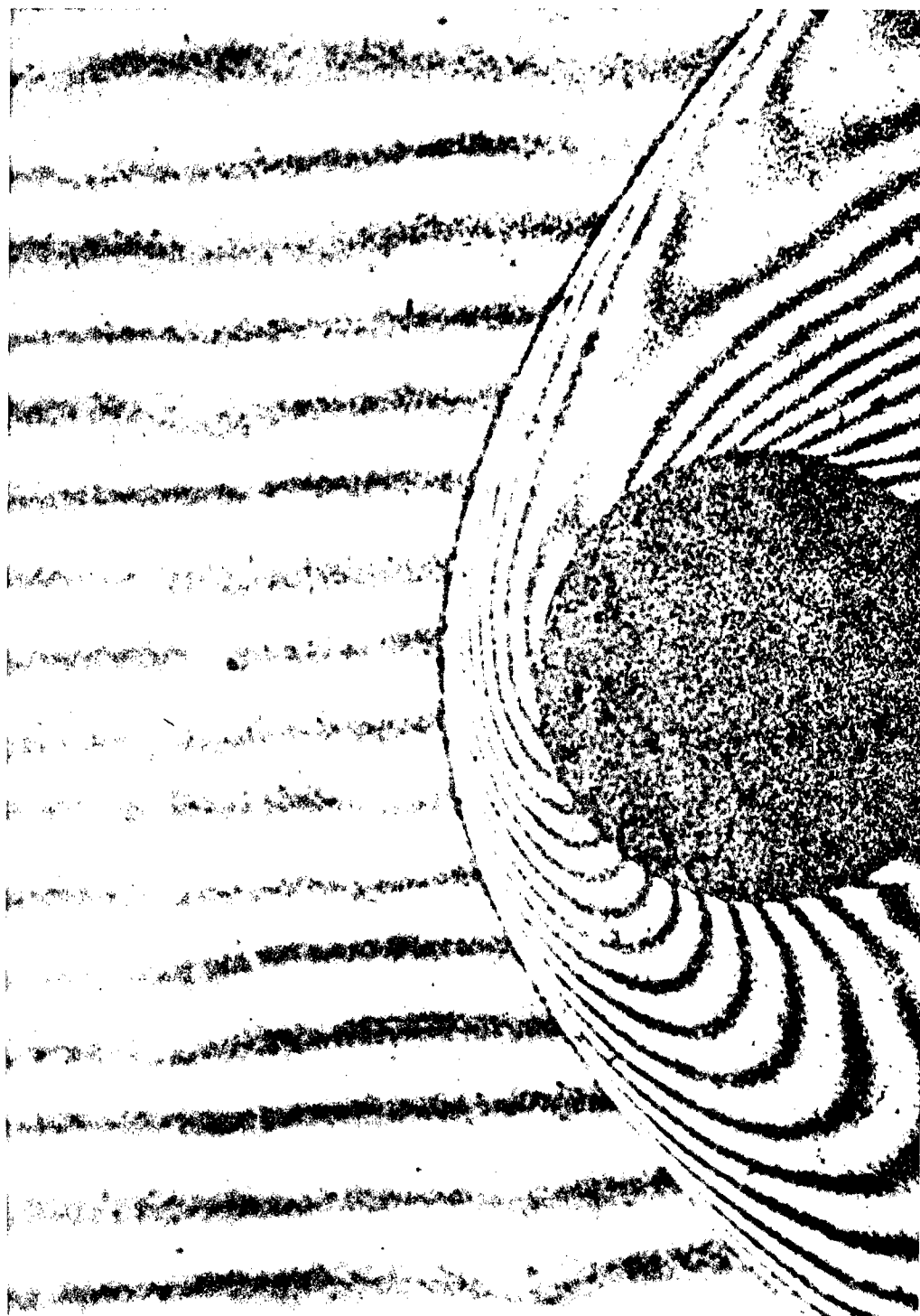
(a) d = $\frac{1}{4}$ inch.

L-62134

Figure 5.- Interferograms of flow around spheres at Mach number 1.81.
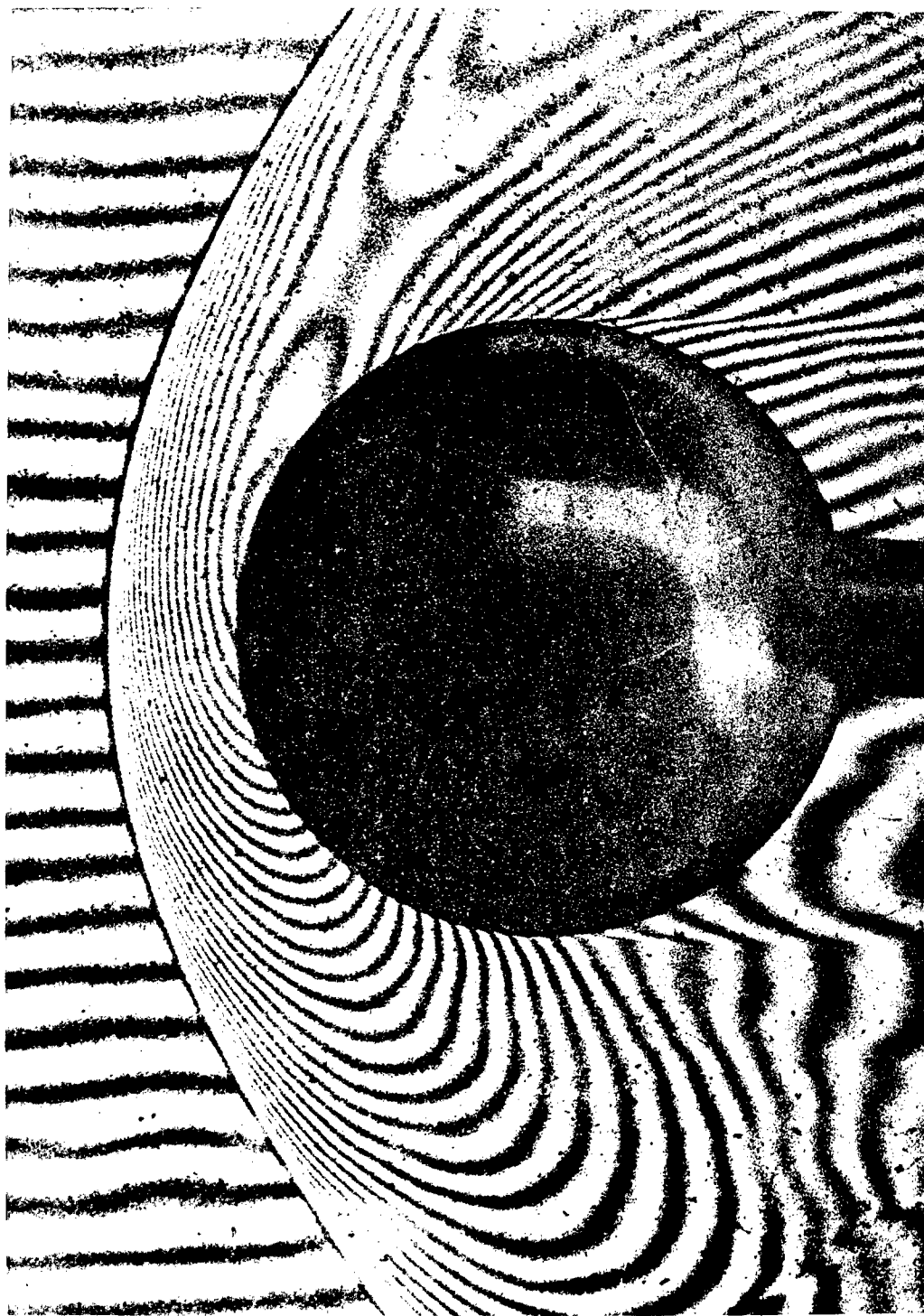
(b) d = $\frac{1}{2}$ inch.

L-62135

Figure 5.- Continued. M = 1.81.
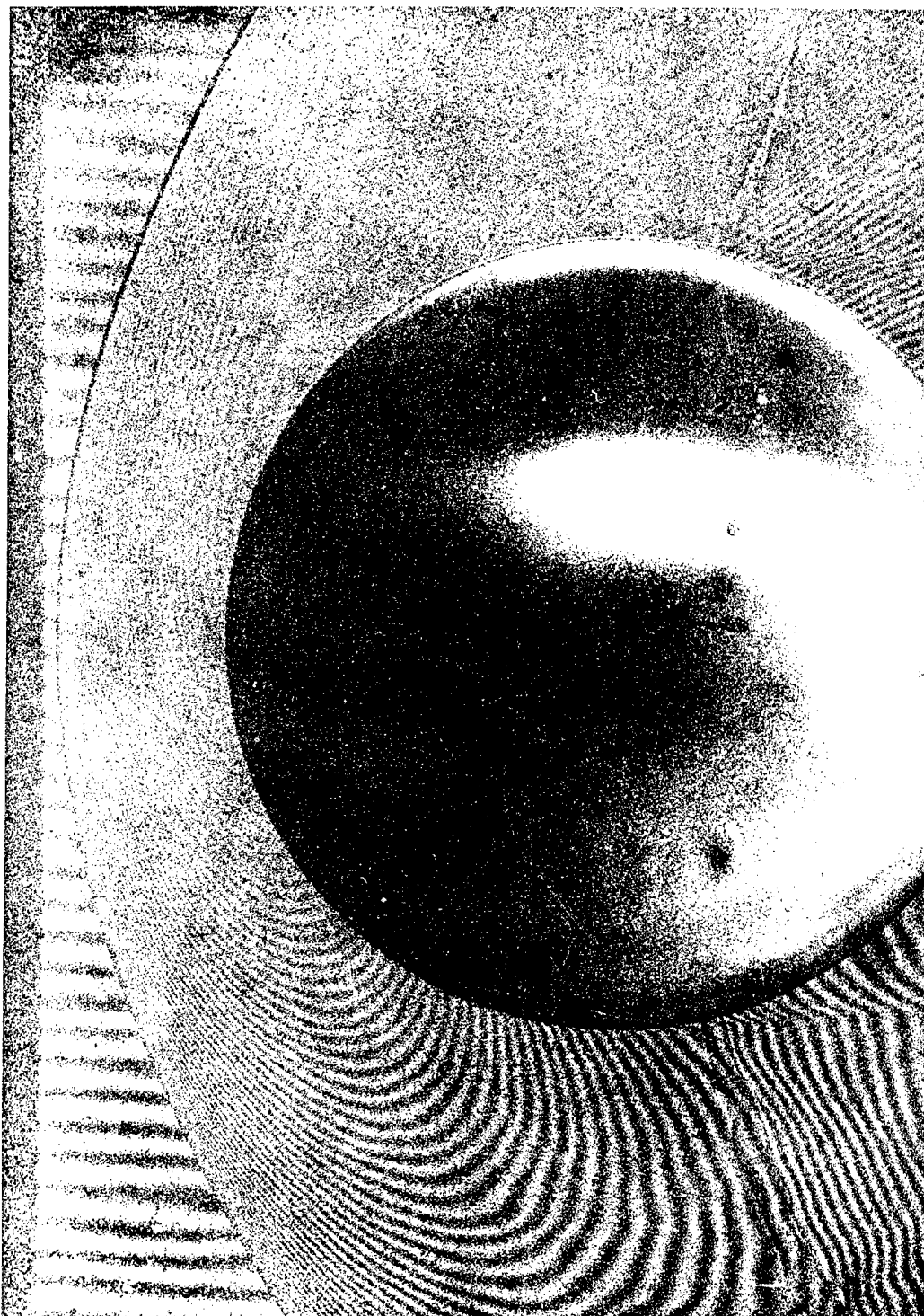
(c)   d = 1 inch.   L-62136

Figure 5.- Concluded. M = 1.81.
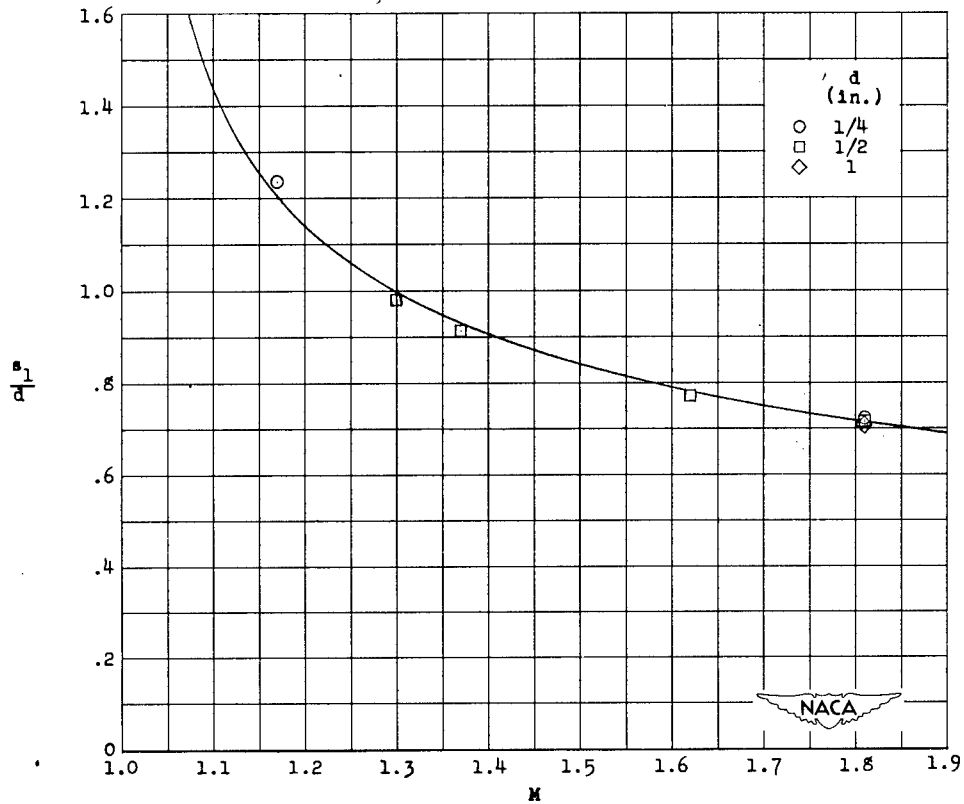
Figure 6.- Variation of $\frac{s_1}{d}$ with M for spheres.
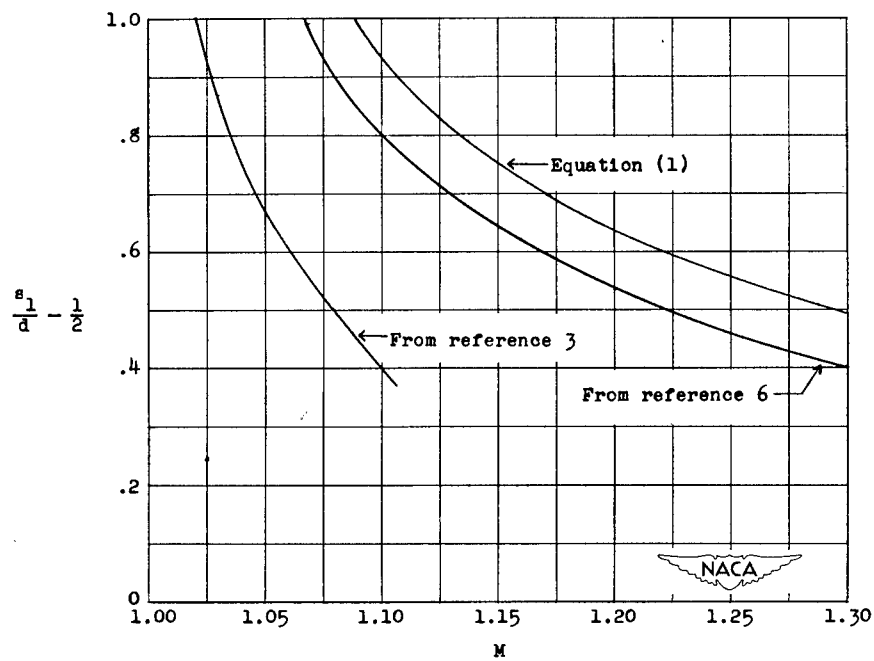
Figure 7.- Comparison of experimental and theoretical results on axial distance of shock wave.
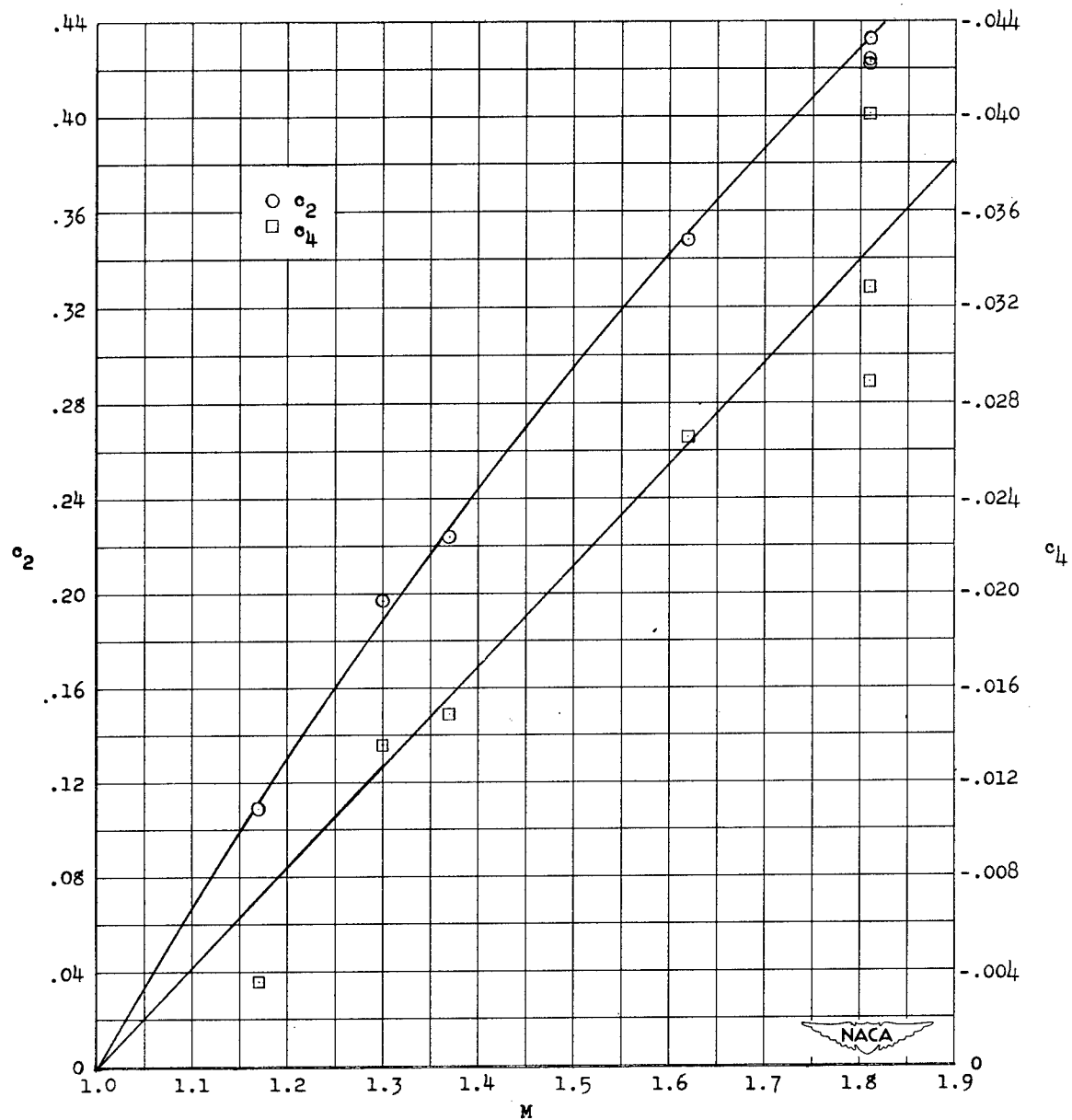
Figure 8.- Variation of coefficients c_2 and c_4 with M for spheres.
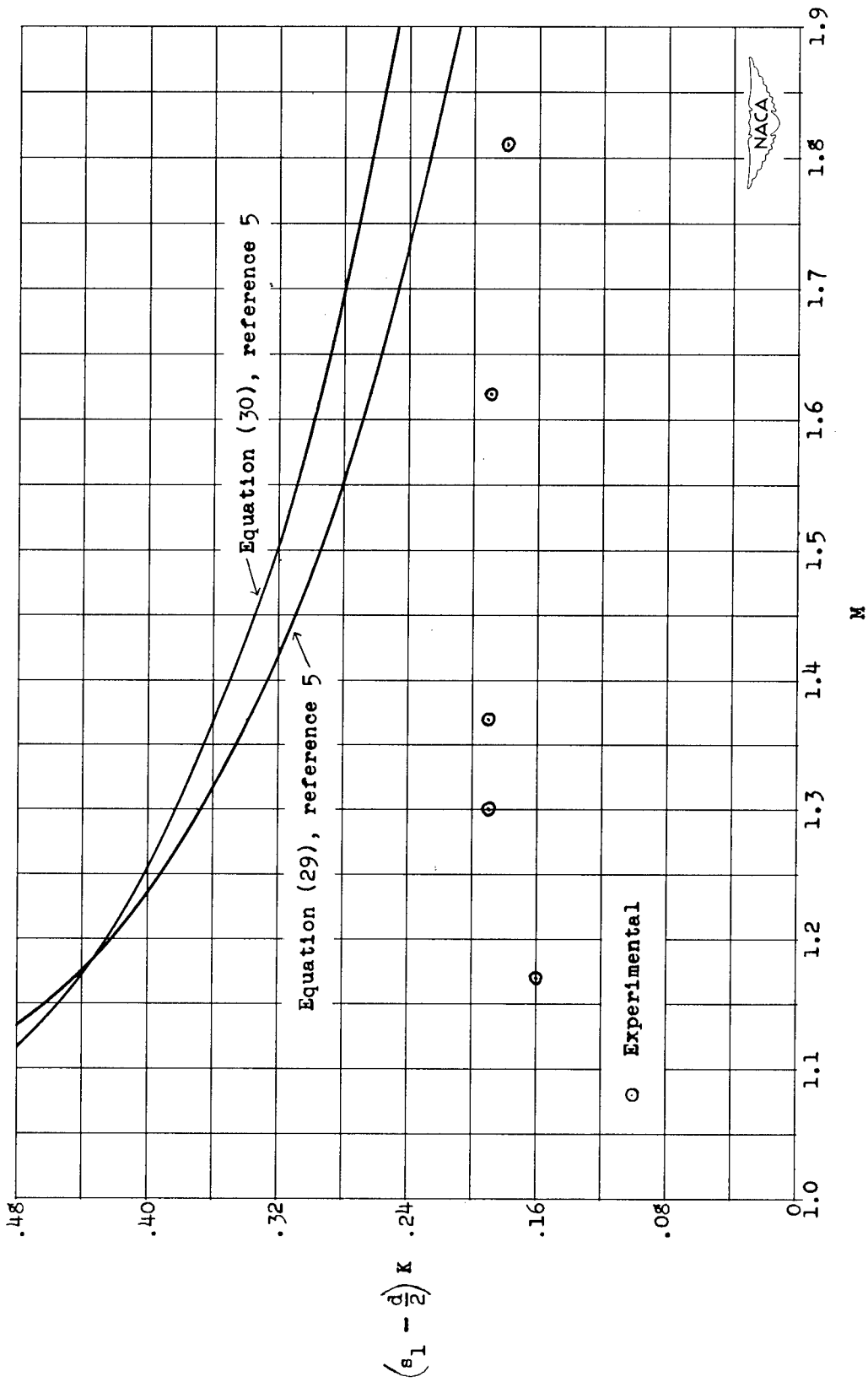
Figure 9.- Comparison of experimental and theoretical results on product of shock-wave distance and curvature.

(a) $\theta = 35^\circ$; d = $\frac{1}{4}$ inch.

L-62137

Figure 10.- Interferograms of flow around cones at Mach number 1.17.

(b) $\theta = 90^\circ$; d = $\frac{1}{4}$ inch.

L-62138

Figure 10.- Concluded. M = 1.17.
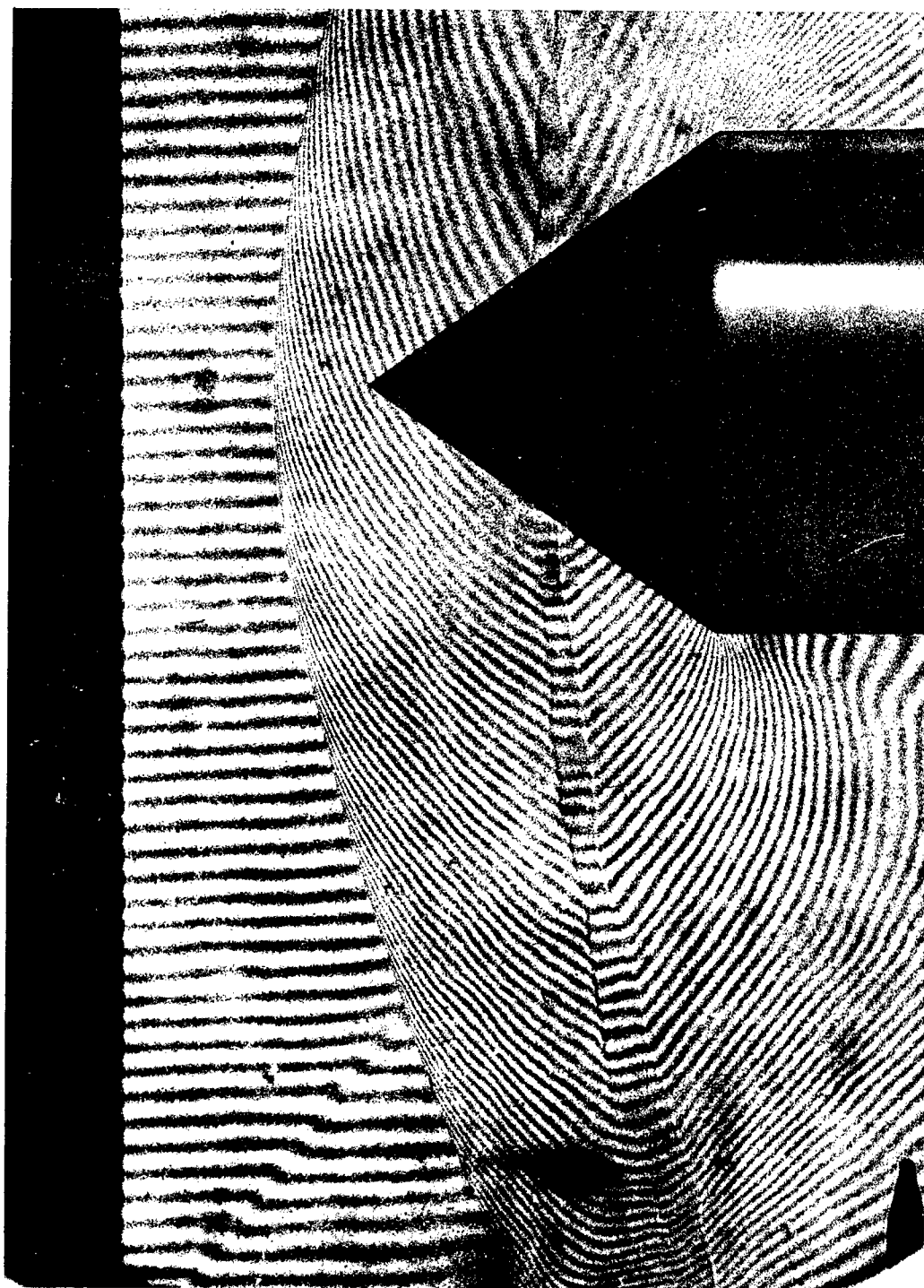
(a) $\theta = 35^\circ$; d = $\frac{3}{4}$ inch.

L-62139

Figure 11.- Interferograms of flow around cones at Mach number 1.30.
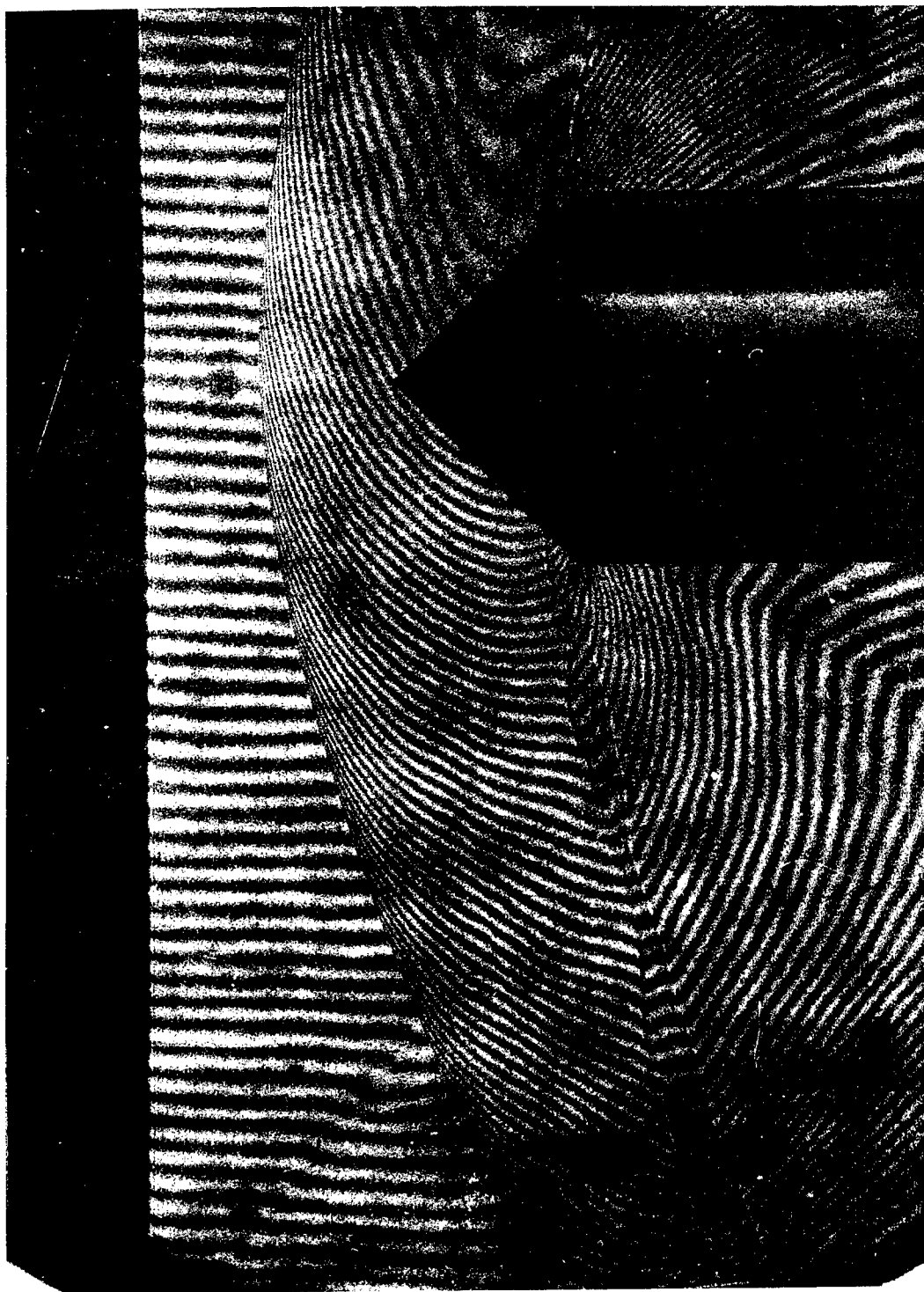
(b) $\theta = 45^\circ$; $d = \dfrac{9}{16}$ inch.

L-62140

Figure 11.- Continued.   M = 1.30.

(c) $\theta = 45°$; $d = \frac{3}{4}$ inch.
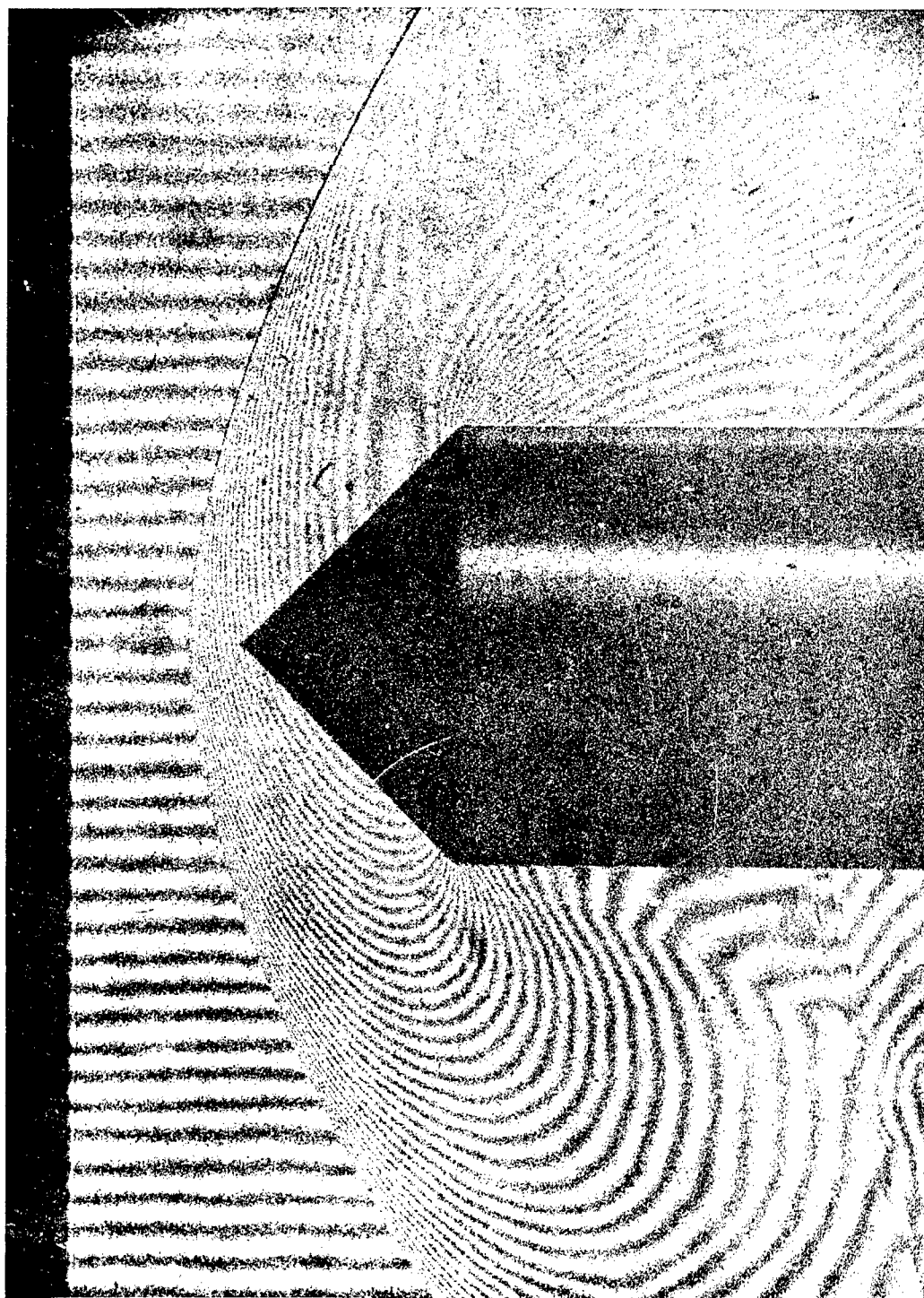
L-62141

Figure 11.- Continued. M = 1.30.
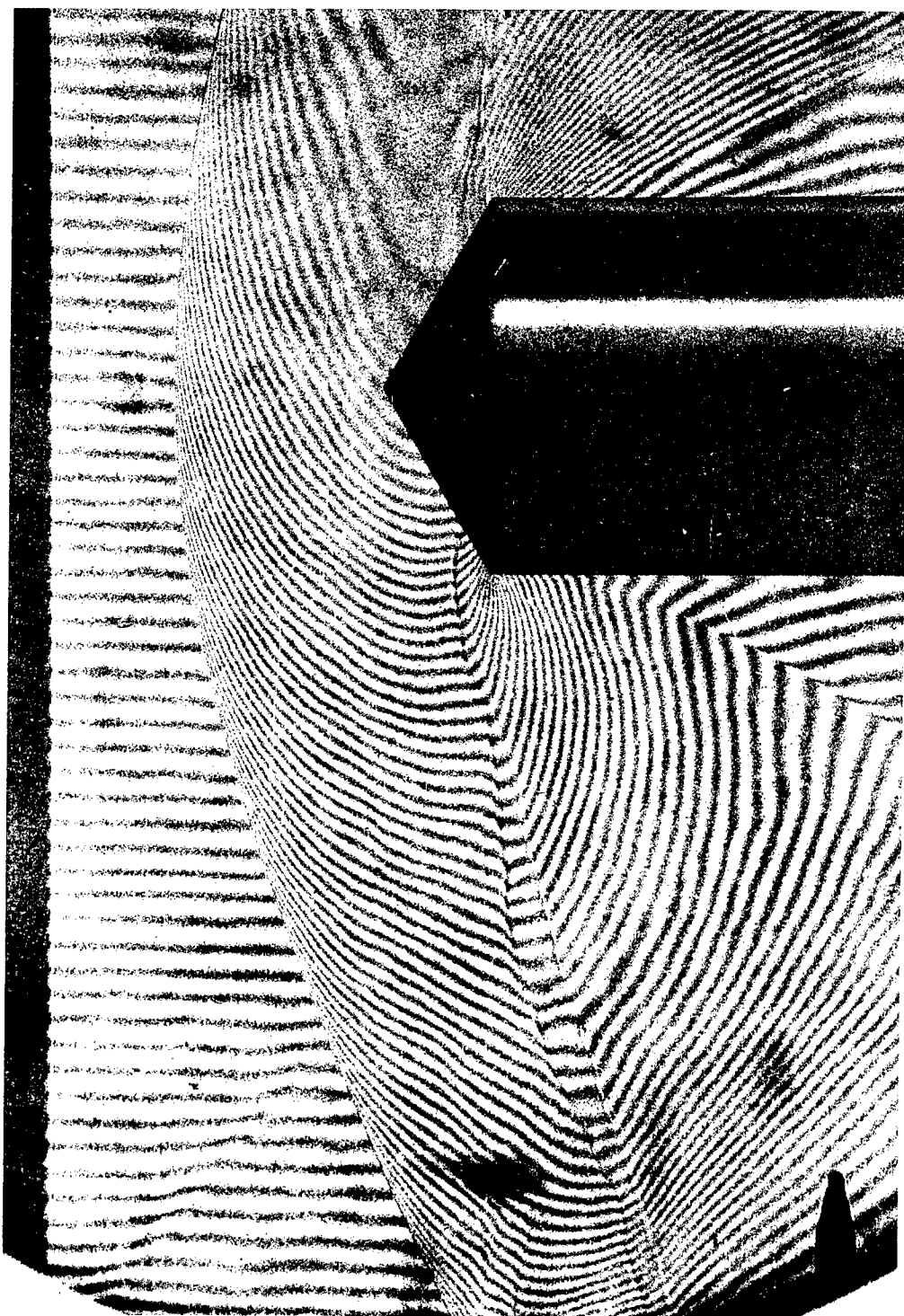
(d) $\theta = 60^\circ$; $d = \frac{9}{16}$ inch.

L-62142

Figure 11.- Continued.   M = 1.30.
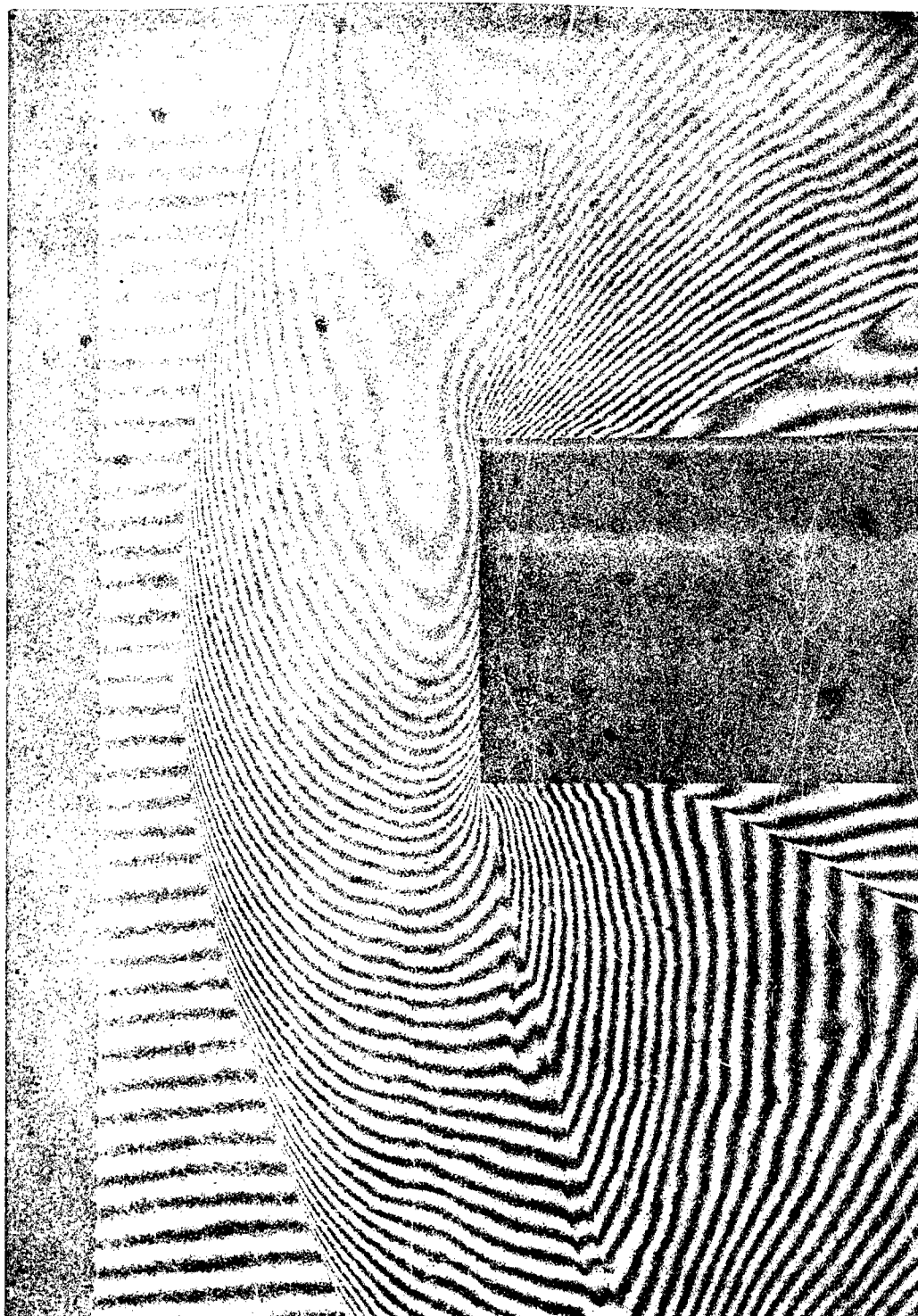
(e) $\theta = 90^{\circ}$; $d = \frac{1}{2}$ inch.

Figure 11.- Concluded.   M = 1.30.
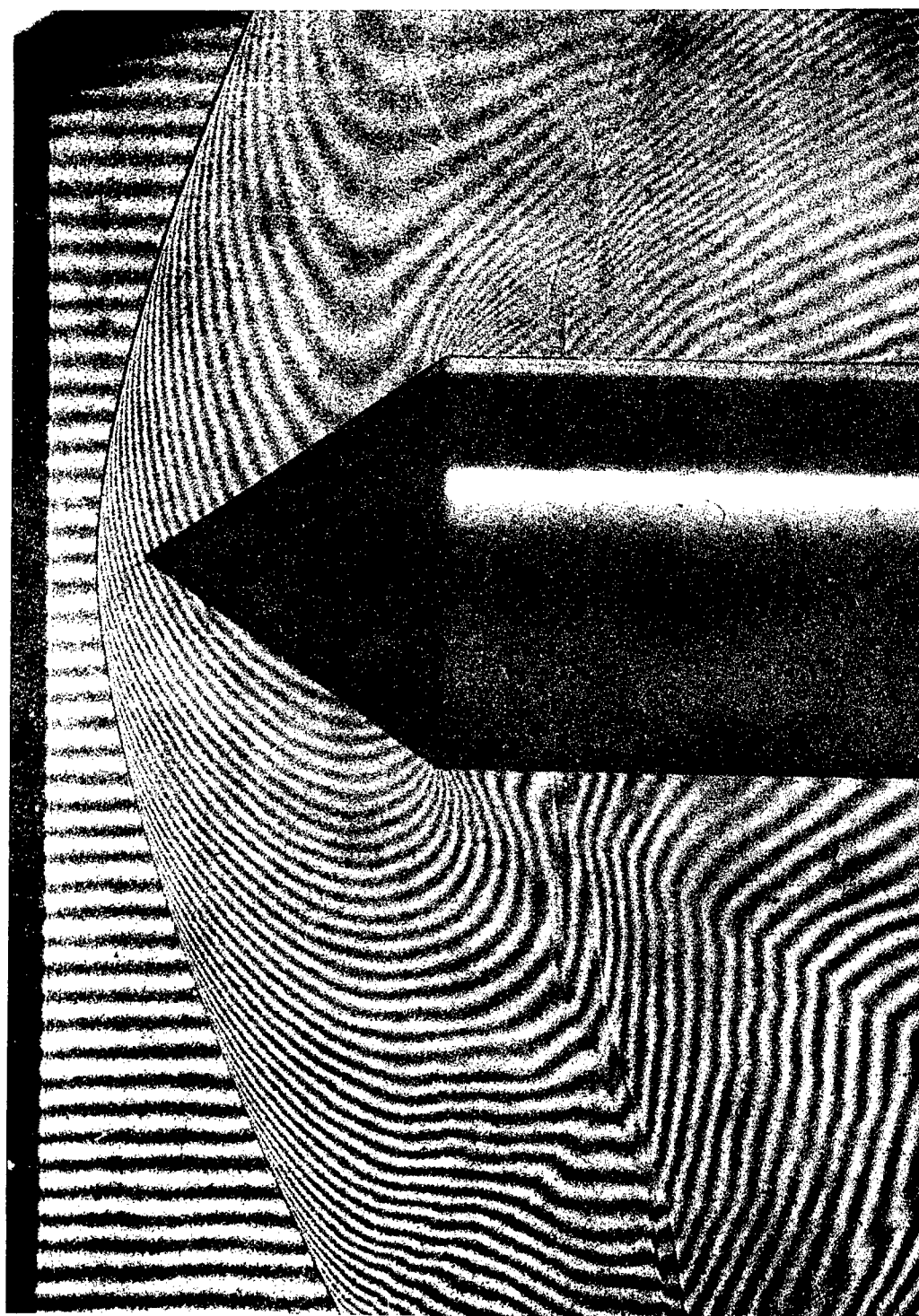
(a) $\theta = 35^\circ$; $d = \frac{9}{16}$ inch.

L-62144

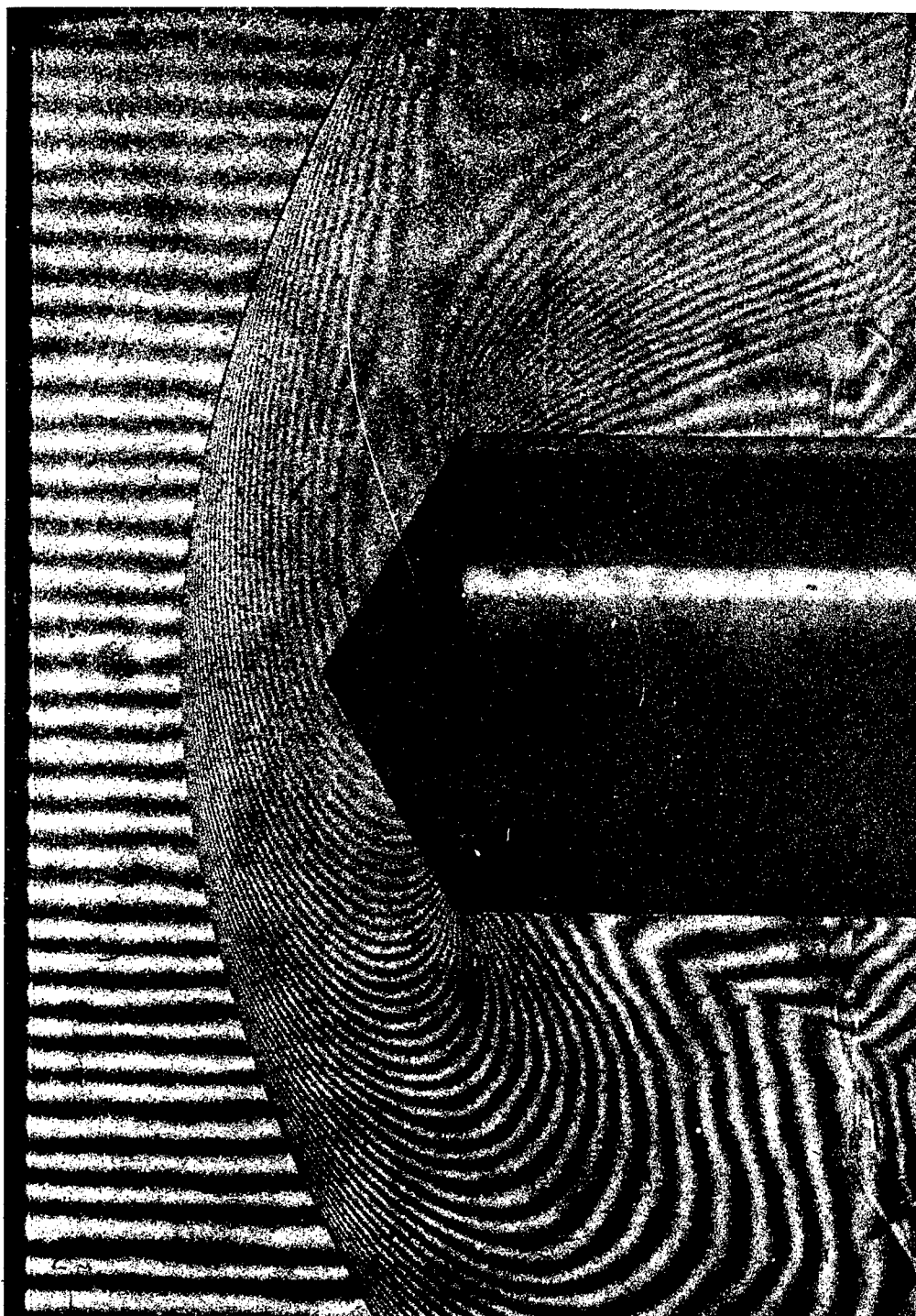Figure 12.- Interferograms of flow around cones at Mach number 1.37.
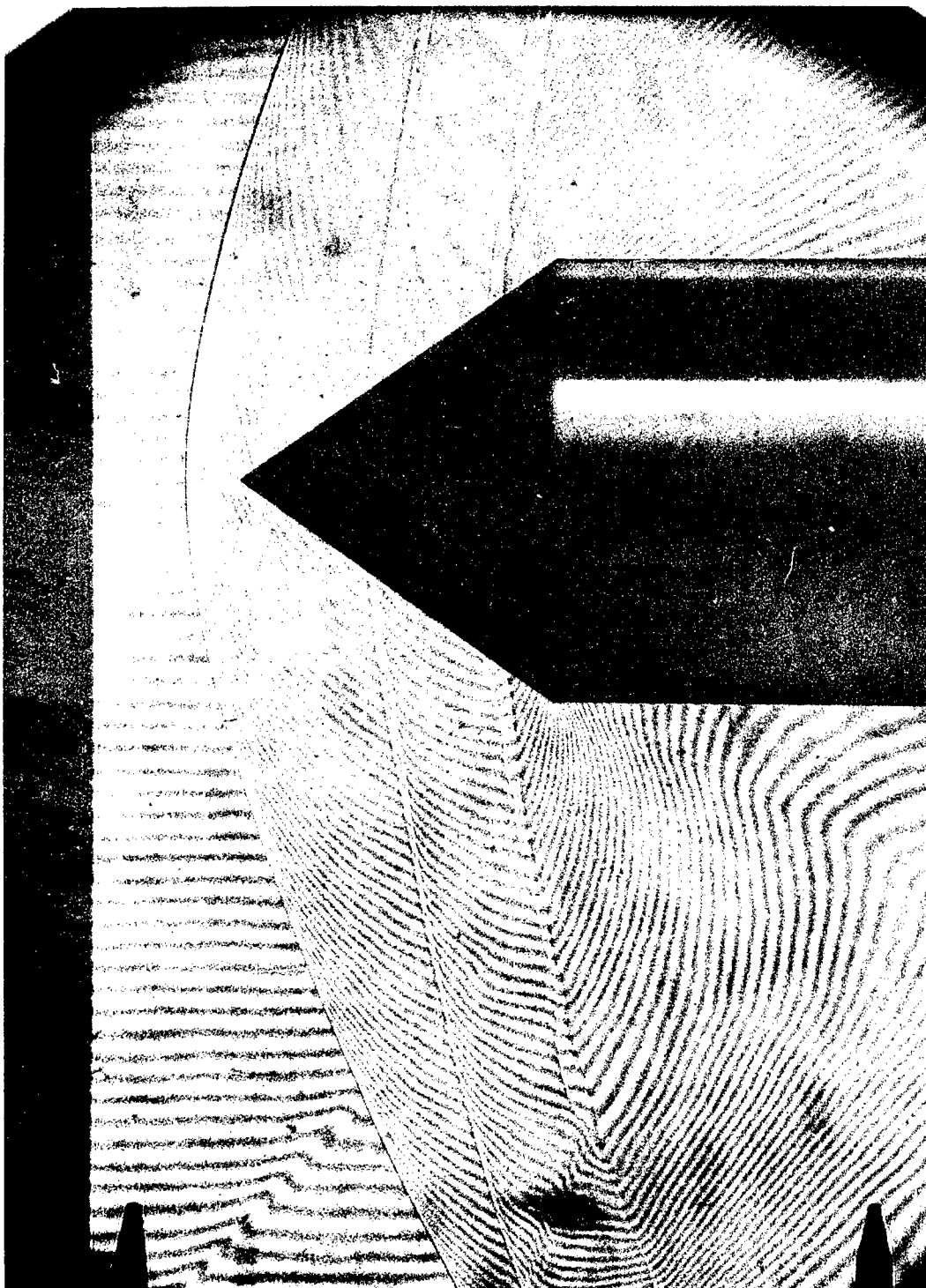
(b) $\theta = 35^{\circ}$; $d = \frac{3}{4}$ inch.
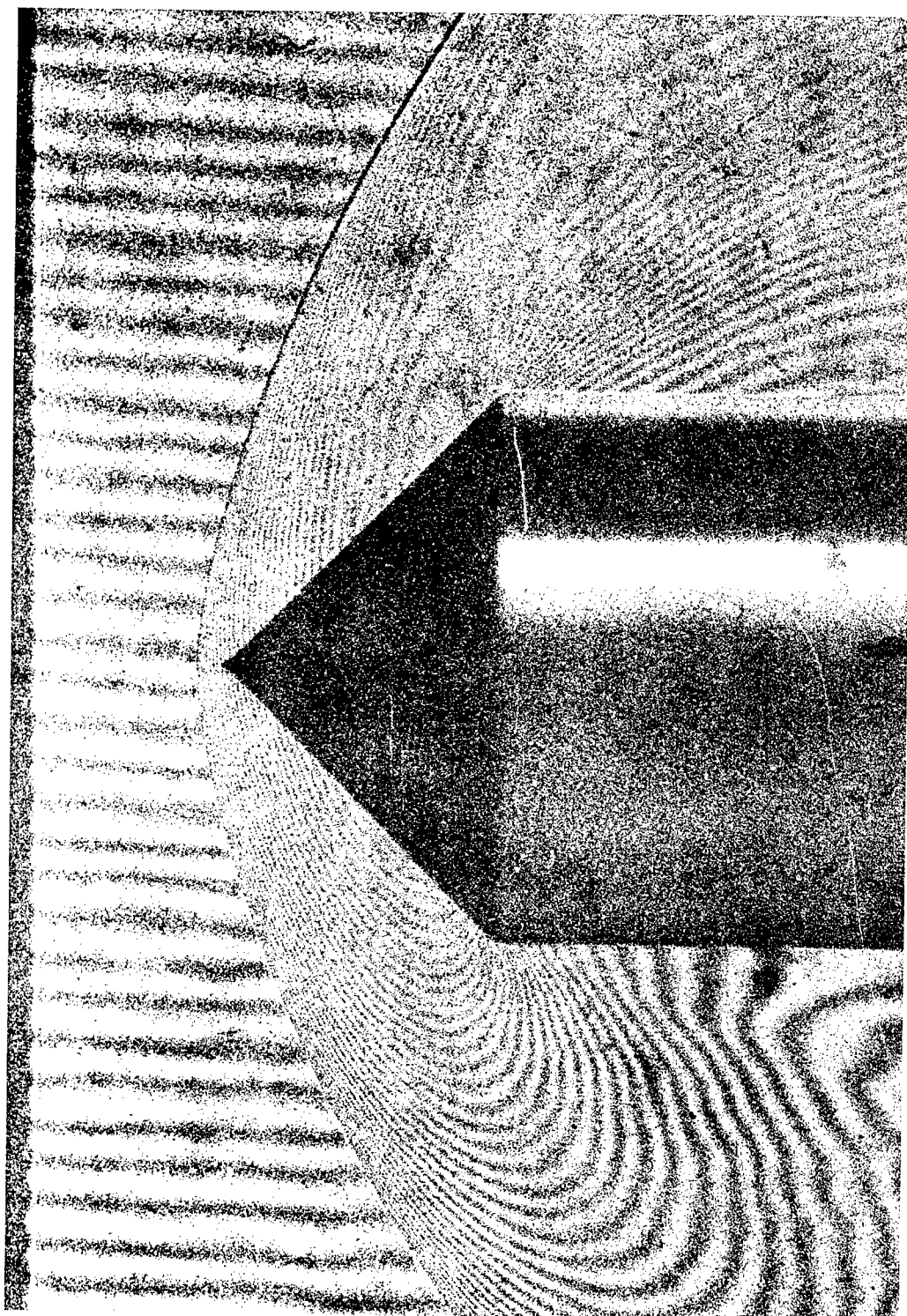
L-62145

Figure 12.- Continued. M = 1.37.
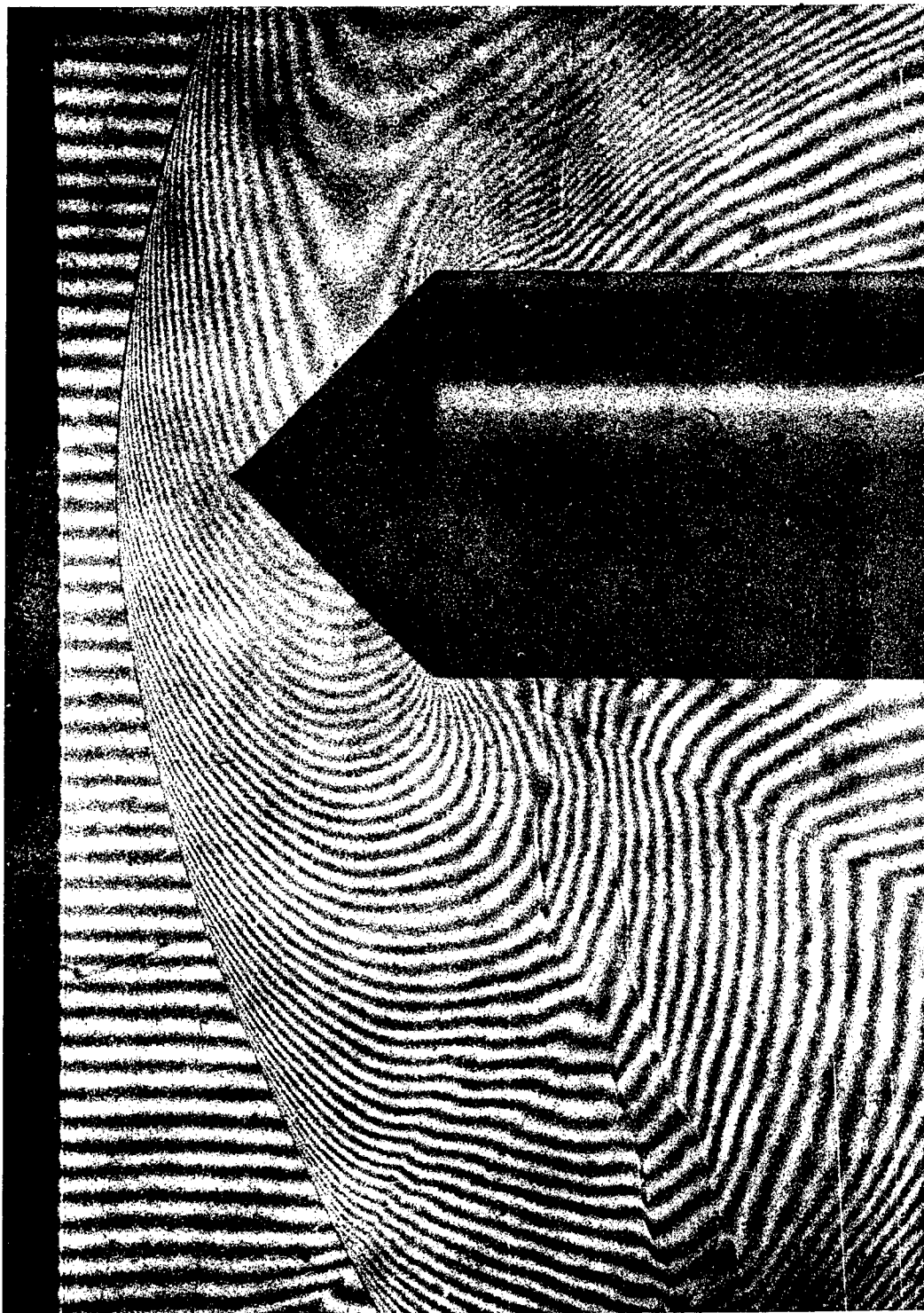
(c) $\theta = 45°$; $d = \dfrac{9}{16}$ inch.

L-62146

Figure 12.- Continued.   M = 1.37.
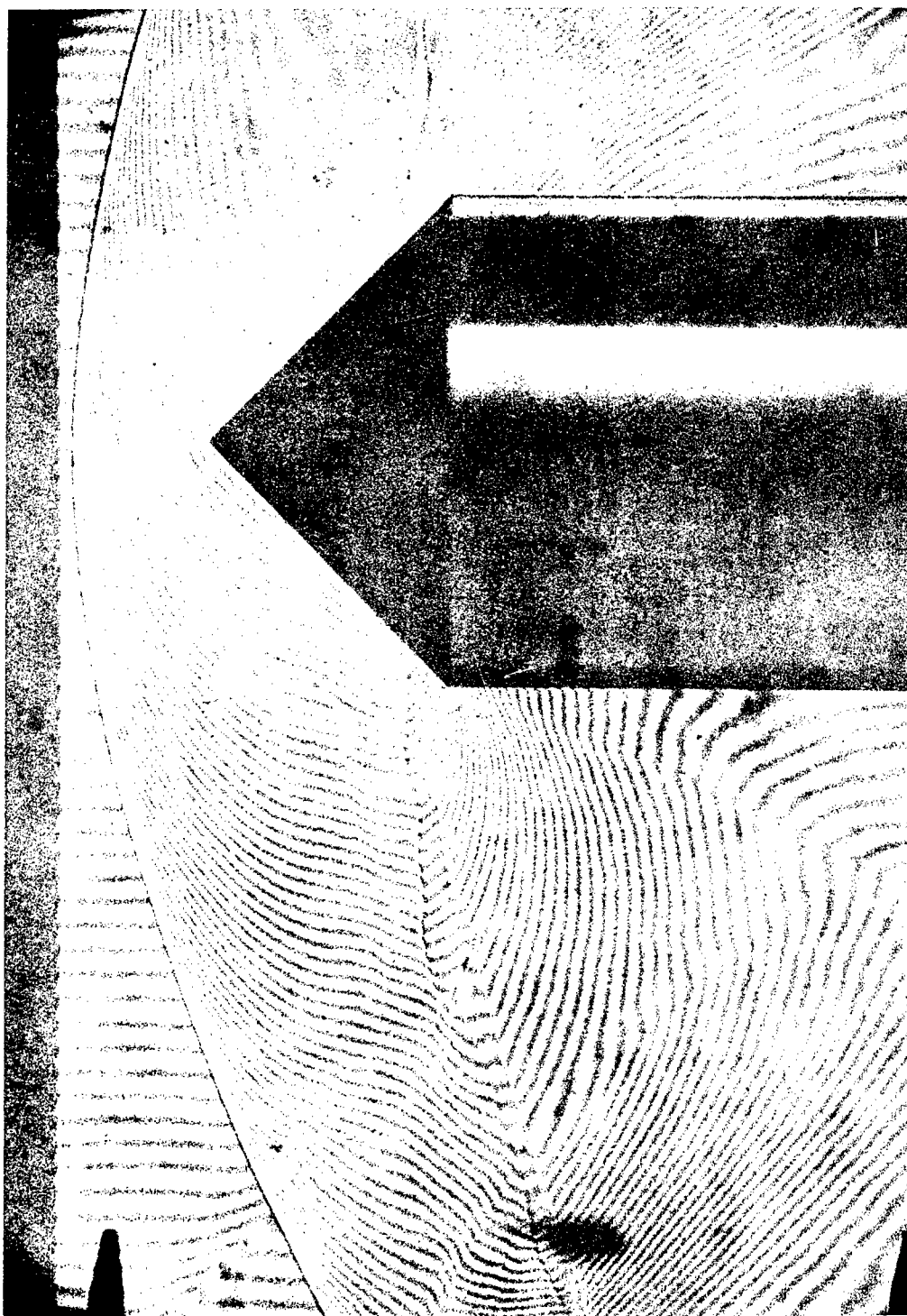
(d) $\theta = 45°$; $d = \frac{3}{4}$ inch.

L-62147

Figure 12.- Continued. $M = 1.37$.
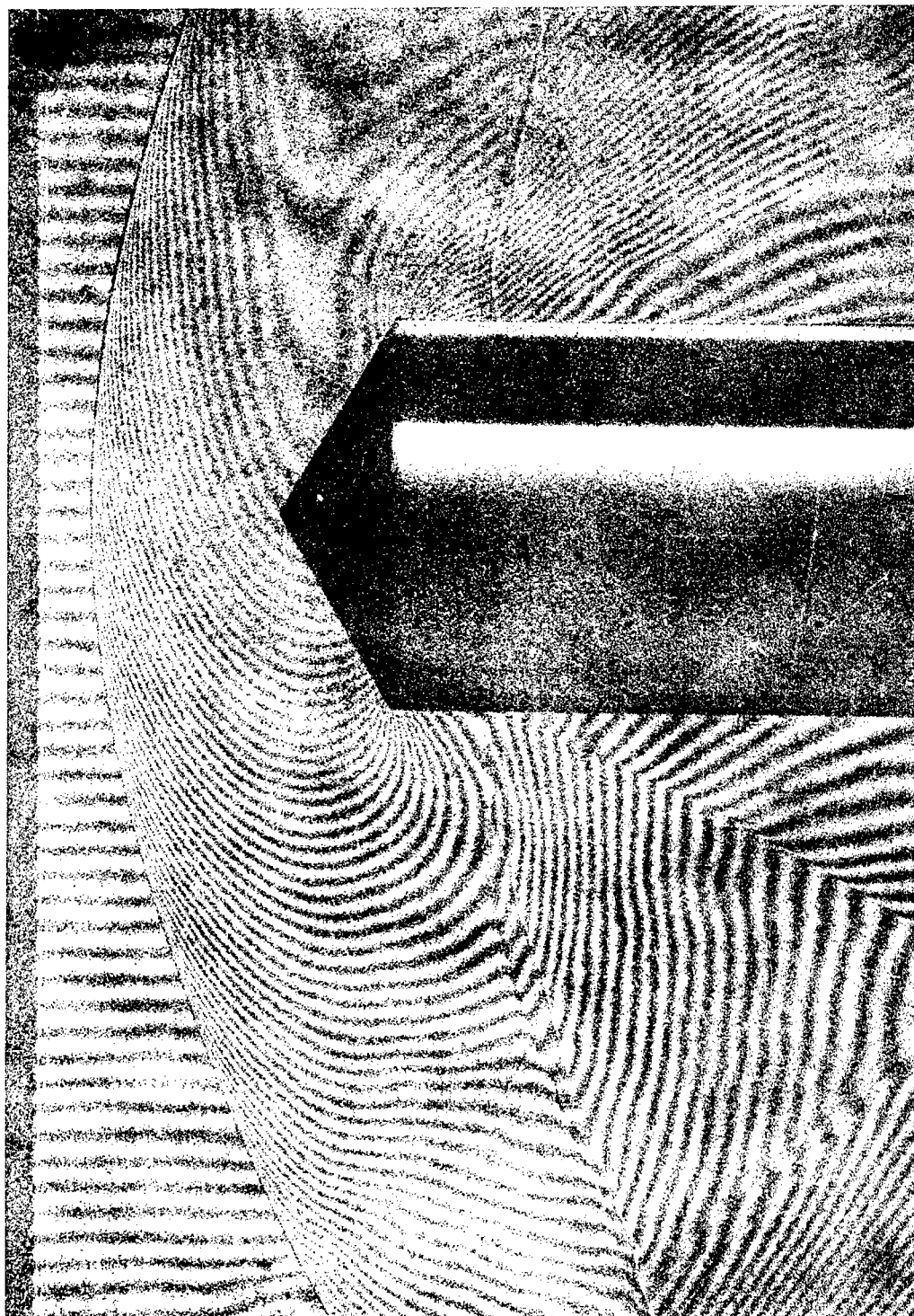
(e) $\theta = 60^{\circ}$; $d = \frac{9}{16}$ inch.

L-62148

Figure 12.- Concluded. M = 1.37.
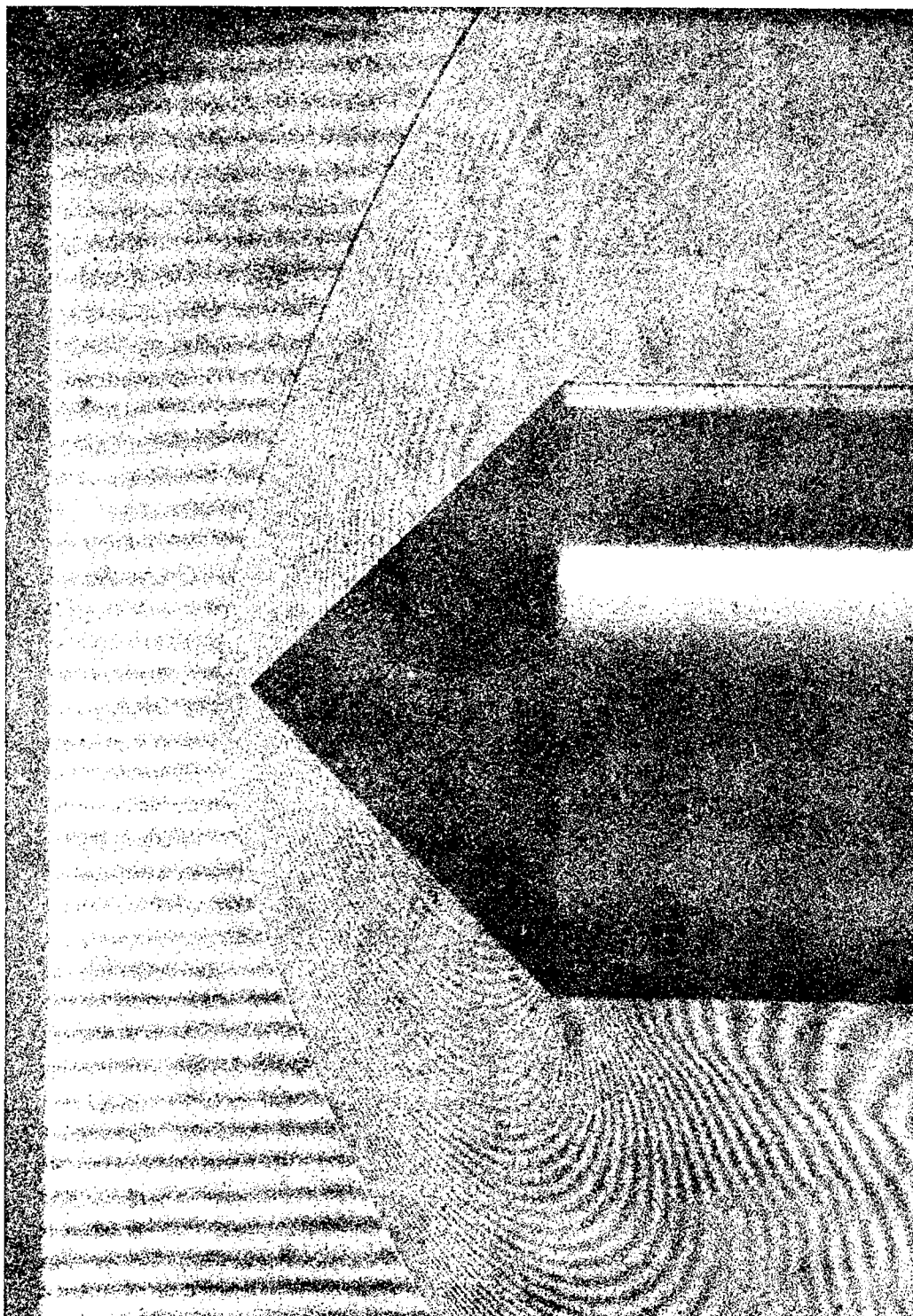
(a) $\theta = 45^{\circ}$; $d = \dfrac{9}{16}$ inch.

L-62149

Figure 13.- Interferograms of flow around cones at Mach number 1.62.
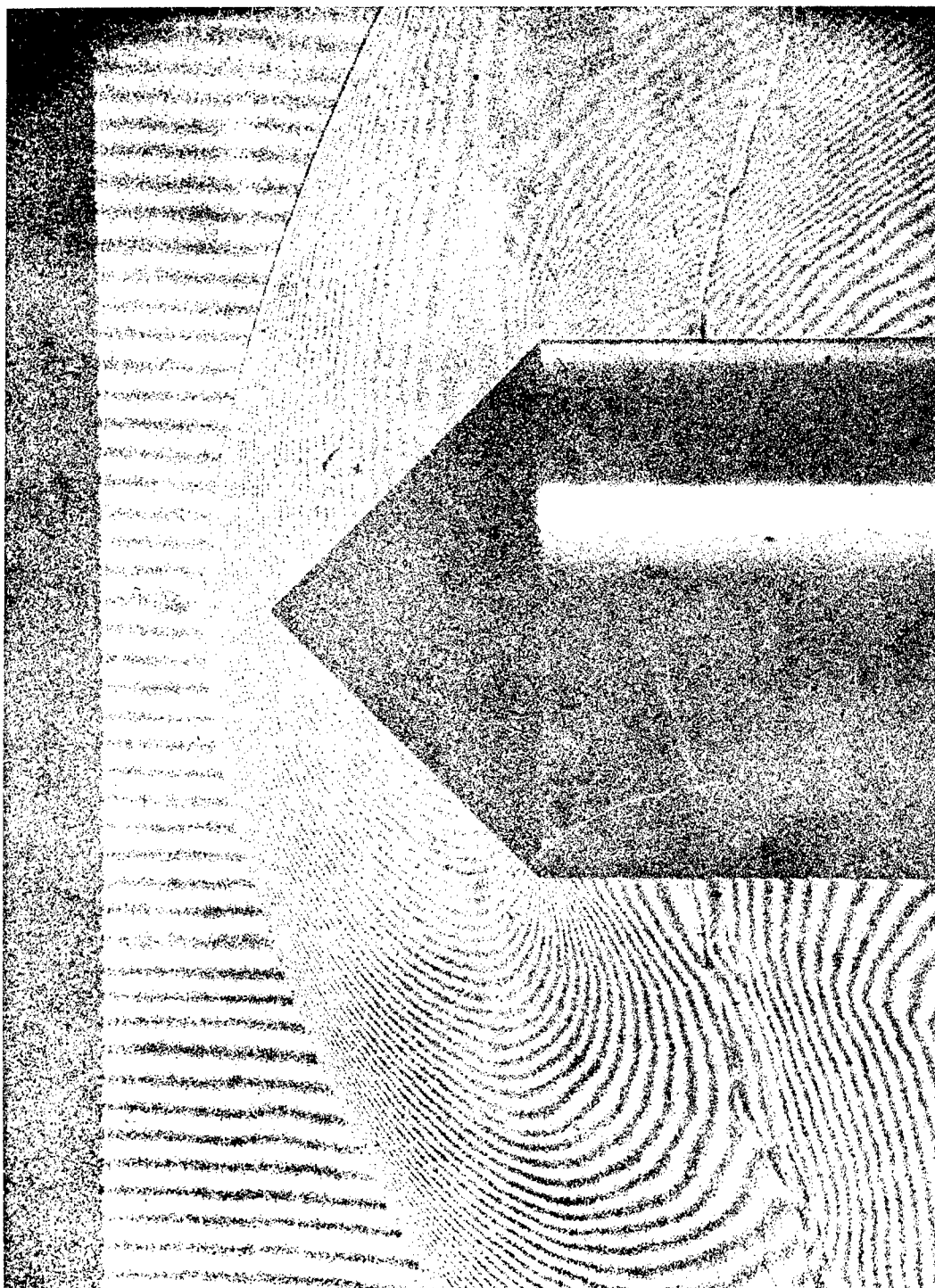
(b) $\theta = 45°$; d = $\frac{3}{4}$ inch.

L-62150

Figure 13.- Continued. M = 1.62.

(c) $\theta = 60°$; $d = \dfrac{9}{16}$ inch.

L-62151

Figure 13.- Concluded. M = 1.62.

(a) $\theta = 45^{\circ}$; $d = \frac{9}{16}$ inch.

L-62152

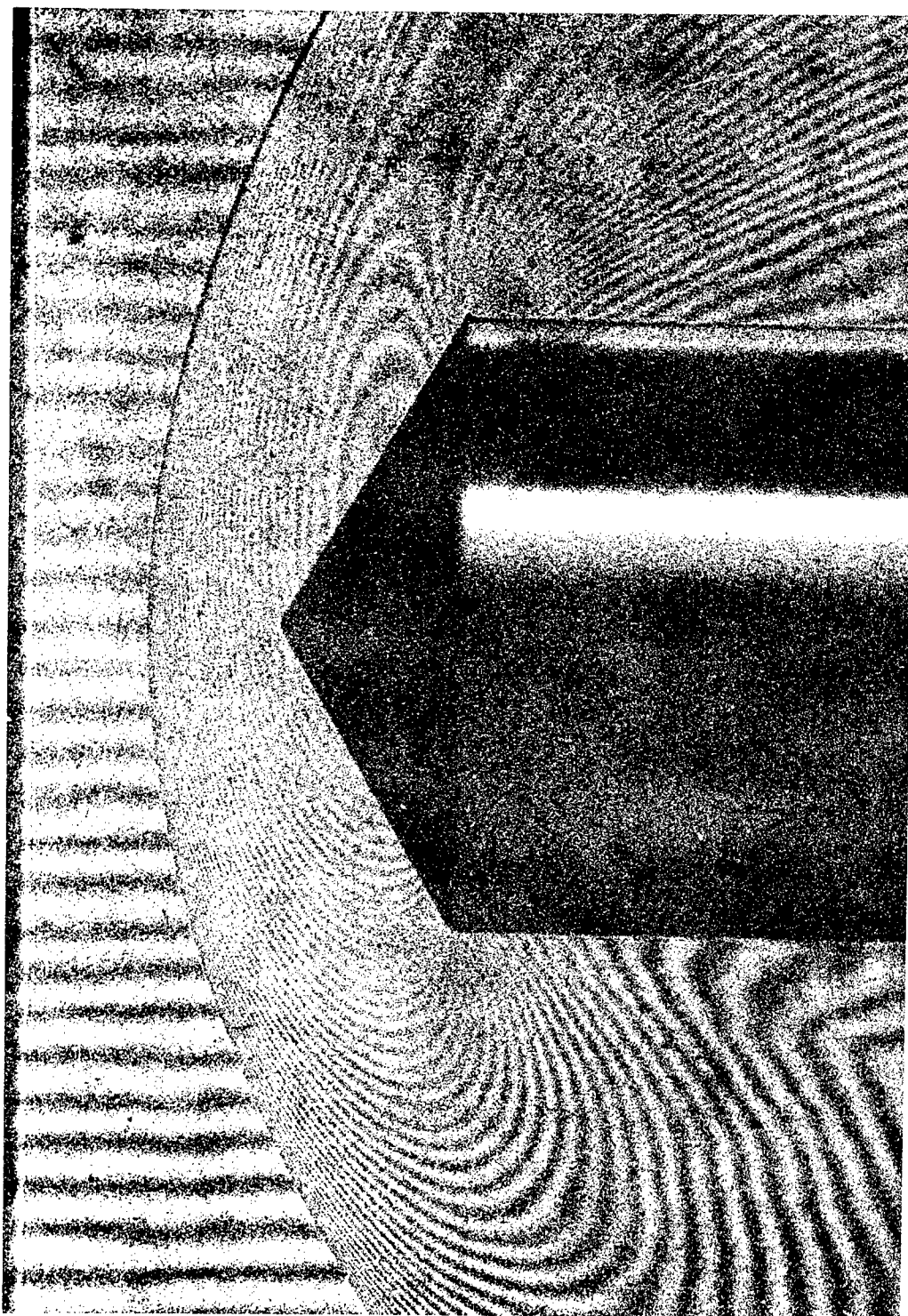Figure 14.- Interferograms of flow around cones at Mach number 1.81.

(b) $\theta = 45°$; $d = \frac{3}{4}$ inch.
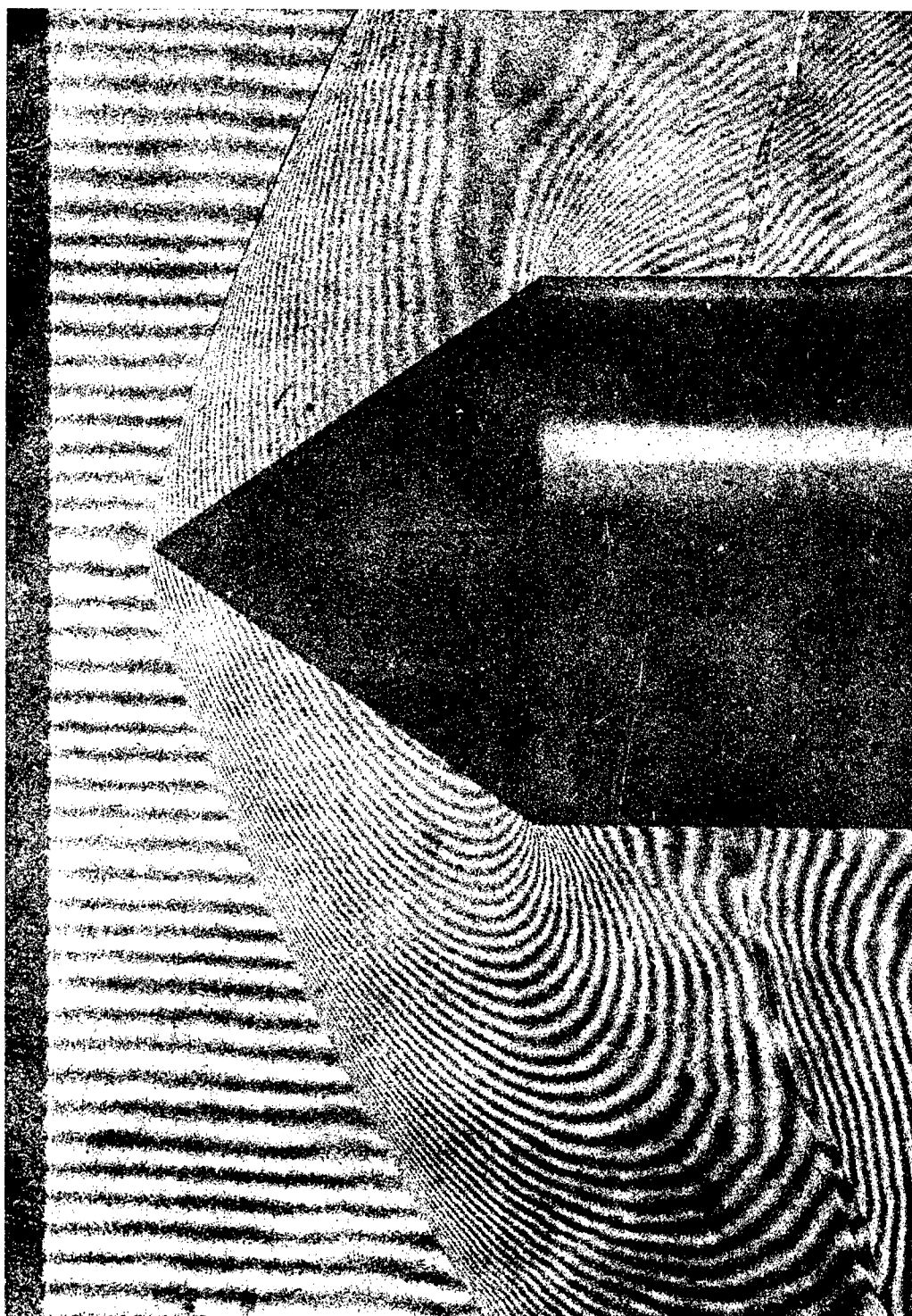
L-62153

Figure 14.- Continued. M = 1.81.

(c) $\theta = 60^{\circ}$; $d = \dfrac{9}{16}$ inch.

L-62154

Figure 14.- Concluded. M = 1.81.

L-62155

Figure 15.- Interferogram of flow around cone showing shock wave nearly attached. $M = 1.62$; $\theta = 35^{\circ}$; $d = \frac{3}{4}$ inch.
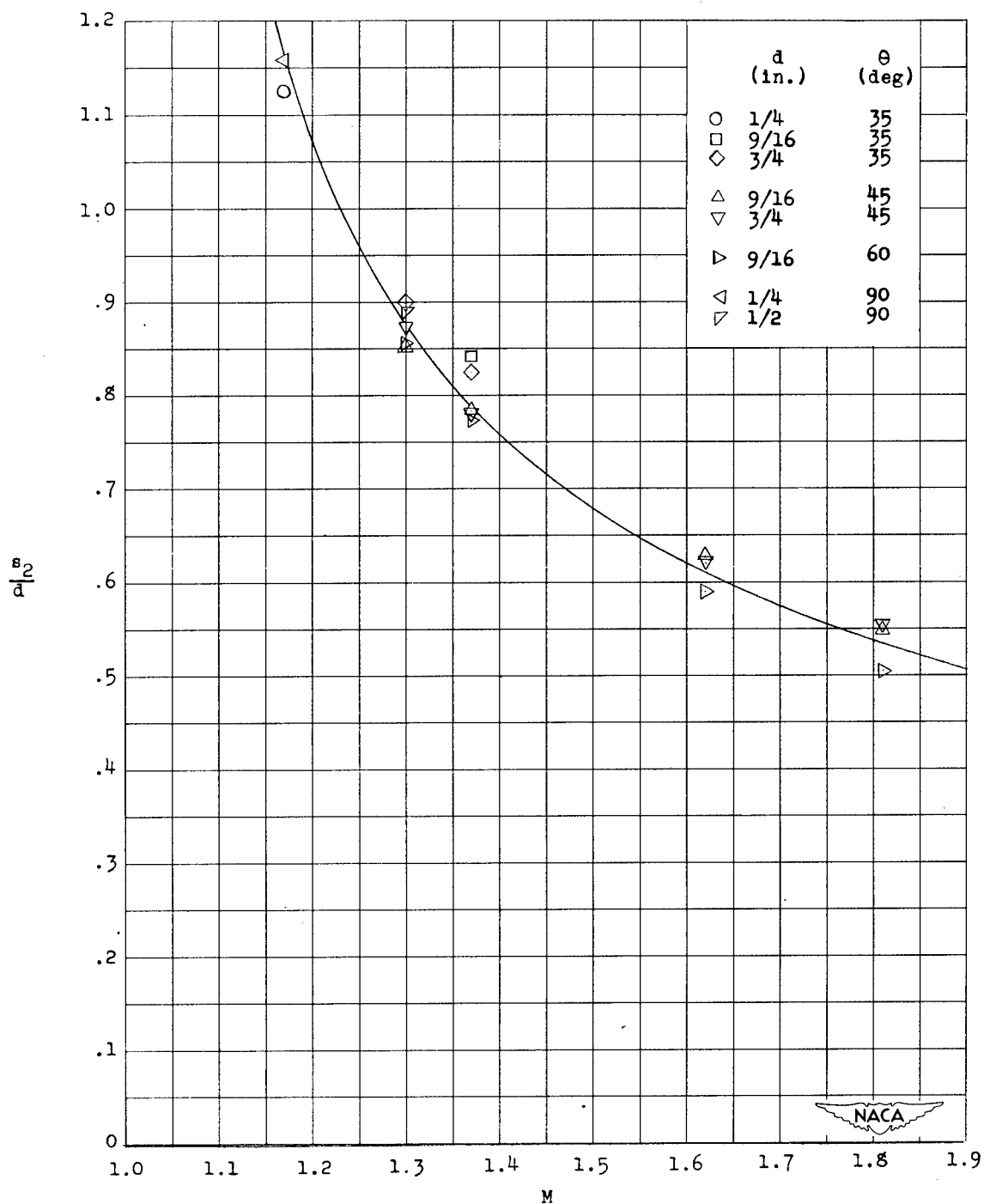
Figure 16.- Variation of $\frac{s_2}{d}$ with M for cones.